Andean Geology 51 (2): 330-356. May, 2024 doi: 10.5027/andgeoV51n2-3686

Geological mapping in the Argentine Frontal Cordillera (~30°30' S) using ASTER images

*Macarena Bertoa del Llano¹, José F. Mescua^{1, 2}, Vanesa D. Litvak^{3, 4}, Lucas D. Lothari¹, Chelsea Mackaman-Lofland⁵, Rebecca A. Vanderleest⁶, Andrés Echaurren¹

- ¹ IANIGLA-CONICET, Av. Ruiz Leal, Parque General San Martín, M5500 Mendoza, Argentina.

 macabertoa@gmail.com, jmescua@mendoza-conicet.gob.ar, lucaslothari@gmail.com, aechaurren@mendoza-conicet.gob.ar
- ² Universidad Nacional de Cuyo, Pedro Jorge Contreras St. 1300, M5502 JMA, Mendoza, Argentina.
- ³ IDEAN UBA-CONICET, 2160 Intendente Güiraldes, Pabellón II, C1428EHA Buenos Aires, Argentina. vane@gl.fcen.uba.ar
- ⁴ Universidad Nacional de Buenos Aires, Intendente Güiraldes 2160, Ciudad Universitaria, C1428EGA, Buenos Aires, Argentina.
- Department of Earth and Environmental Sciences, Denison University, 100 W College St, Granville, Ohio, USA. mackamanloflandc@denison.edu
- ⁶ Department of Life, Earth, and Environmental Sciences, West Texas A&M University, 2501 4th Ave, TX 79016, Canyon, TX, USA. rvanderleest.wtamu@gmail.com
- * Corresponding author: macabertoa@gmail.com

ABSTRACT. The eastern flank of the Argentine Frontal Cordillera at ~30°30'S is a remote area with rugged topography and high elevations that hinder geological field mapping. This task is also challenging because several outcrops are dominated by Permian-Triassic and Cenozoic volcanic rocks of intermediate to acid compositions with scarce geochronological age constraints. In this work, we use ASTER (Advanced Spaceborne Thermal Emission and Reflection Radiometer) data to clarify the structural and stratigraphic framework of the region. Visible and near infrared (VNIR) and shortwave infrared (SWIR) band combinations, integrated with field observations, are effective in identifying first-order geological features. In addition, the Semi-Automatic Classification Plugin (SCP; a free open-source plugin for QGIS) is capable of discriminating lithological units and is especially useful to visualize their distribution. Results presented here allow us to characterize Permian-Triassic and Cenozoic units, propose tentative correlations between the Permian-Triassic rocks, and outline major tectonic structures in the study area. This work demonstrates the capability of ASTER data to improve geological mapping, especially in those places where field work is difficult.

Keywords: Remote sensing, Geological mapping, Frontal Cordillera, Choiyoi Group, Olivares Group.

RESUMEN. Mapeo geológico de la Cordillera Frontal de Argentina (~30°30' S) mediante imágenes ASTER. El flanco oriental de la Cordillera Frontal argentina a los ~30°30' S es una zona remota de relieve escarpado y grandes elevaciones que complican el mapeo geológico de campo. Esta tarea también se ve dificultada debido a que gran parte de los afloramientos están dominados por rocas volcánicas del Pérmico-Triásico y Cenozoico, son de composiciones intermedias a ácidas, y hay escasos estudios geocronológicos. En este trabajo, se utilizan imágenes ASTER (*Advanced Spaceborne Thermal Emission and Reflection Radiometer*) con el objetivo de clarificar el marco estructural y estratigráfico de la región. Las combinaciones de bandas VNIR (*Visible and Near Infrared*) y SWIR (*Shortwave Infrared*), integradas con observaciones de campo, son efectivas en el reconocimiento de rasgos geológicos de primer orden. Por otro lado, la herramienta de clasificación SCP (*Semi-Automatic Classification Plugin*) es capaz de discriminar unidades litológicas y es particularmente útil para visualizar su distribución. Los resultados obtenidos permiten caracterizar las unidades Pérmico-Triásicas y Cenozoicas, proponer correlaciones tentativas entre las rocas de dichos períodos, y trazar las principales estructuras tectónicas dentro de la zona de estudio. La presente contribución evidencia la capacidad de las imágenes ASTER en el mapeo geológico, especialmente en aquellos lugares donde el trabajo de campo es difícil de llevar a cabo.

Palabras clave: Sensores remotos, Mapeo geológico, Cordillera Frontal, Grupo Choiyoi, Grupo Olivares.

1. Introduction

The Andes are one of the most important subduction-related mountain ranges worldwide, being the subject of numerous field studies and geological investigations. Due to their remoteness and rough topography, there are still several regions in the Andes where geological field mapping is limited, leaving important aspects related to their configuration and evolution poorly understood and highly debated. In such regions, remote sensing analyses using satellite imagery may be an alternative and powerful tool for preliminary lithological and structural mapping, as has been implemented elsewhere in the world (*e.g.*, Ninomiya *et al.*, 2005; Watts *et al.*, 2005; Mars

and Rowan, 2006; Ourhzif *et al.*, 2019; Pour *et al.*, 2019; Beygi *et al.*, 2020; Kamel *et al.*, 2022; Baid *et al.*, 2023; Marzouki and Dridri, 2023; Ouhoussa *et al.*, 2023).

At ~30°30'S, the core of the Andes is represented by the Frontal Cordillera (Fig. 1A-B), a prominent topographic feature that reaches elevations of >6,000 m a.s.l. (Moscoso and Mpodozis, 1988). This unit is a thick-skinned thrust system that exposes Paleozoic and Lower Triassic rocks, covered by Mesozoic and Cenozoic volcanic and sedimentary sequences (Caminos, 1979; Moscoso and Mpodozis, 1988; Ramos, 1999; Martínez *et al.*, 2018). One of the main features of the Frontal Cordillera is its extensive Permian-Triassic plutonic and

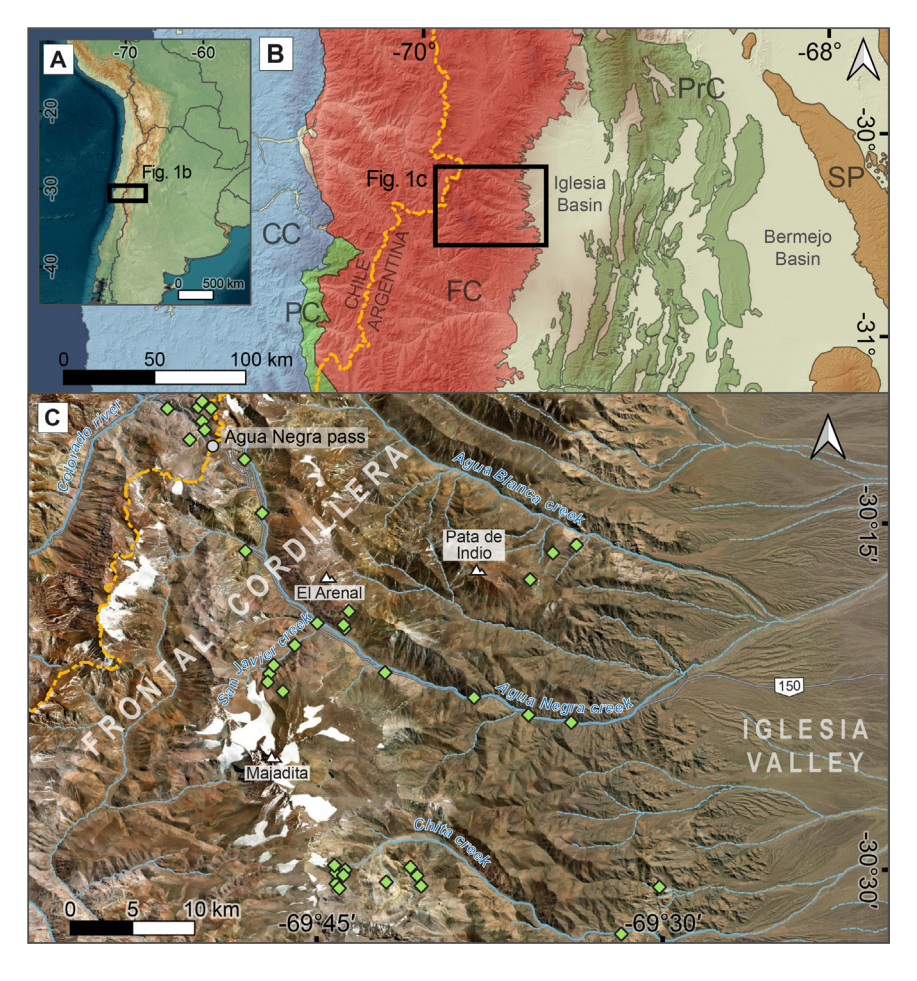


FIG. 1. A-B. Relief map of South America and regional map showing the location of the study area in the eastern Frontal Cordillera (black rectangle). Abbreviations: CC: Coastal Cordillera, PC: Principal Cordillera, FC: Frontal Cordillera, PrC: Precordillera, SP: Sierras Pampeanas. C. Satellite image of the study area, taken from ESRI Online World Imagery base map. Green diamonds indicate field verification points.

volcanic rocks record (Ramos, 1999). The volcanic sequences are grouped into the Choiyoi Group and are interpreted to represent the extrusive products of a significant and widespread magmatism that took place between ca. 286 and 247 Ma (Sato et al., 2015). Key tectonic and geodynamic aspects of this magmatic event remain debated (Mpodozis and Kay, 1990, 1992; Llambías and Sato, 1995; Kleiman and Japas, 2009; Rocher et al., 2015; Coloma et al., 2017; del Rey et al., 2019; Bastías-Mercado et al., 2020; Oliveros et al., 2020; Gianni and Navarrete, 2022), due in part to the relatively low amount of available data from Choiyoi volcanic rocks and their intrusive equivalents (Bastías-Mercado et al., 2020). At ~30°30' S, particularly in the Argentine Frontal Cordillera, outstanding questions persist regarding the chronostratigraphic designations of the Choiyoi Group, mostly due to the difficulties in field mapping and the few geochronological data available. In addition, the poorly studied Cenozoic volcanic units are sometimes hard to differentiate from the Permian-Triassic volcanics. These rocks, erupted between Oligocene and Pliocene times, are also key to understanding the timing of Andean orogenesis and crustal thickening in this region. A better knowledge of their stratigraphy and distribution can provide more precise models of Andean magmatism and mountain building.

The aim of this study is to clarify the geological framework of the Argentine Frontal Cordillera at ~30°30' S through remote sensing. For this purpose, we use ASTER (Advanced Spaceborne Thermal Emission and Reflection Radiometer) multispectral images due to their wide wavelength coverage and sensitivity in the different spectral regions (Abrams and Hook, 1995; Rowan and Mars, 2003; Abrams and Yamaguchi, 2019). Although previous studies have also used multispectral image processing at similar latitudes in the Frontal Cordillera (Delendatti, 2003; Pérez et al., 2010; Testa et al., 2018; Cócola et al., 2022), most of them focused on the recognition of alteration mineral associations in mining prospects. In this work, ASTER multispectral imagery analysis is used for lithological mapping. In particular, we aim at differentiating units within the Permian-Triassic and Cenozoic record, formed predominantly by intermediate to acid volcanic rocks and subordinate sedimentary deposits. Our results contribute to a better understanding of the geology of the Argentine Frontal Cordillera and allow us to characterize

Permian-Triassic and Cenozoic units, propose tentative correlations between the Permian-Triassic rocks, and outline the major tectonic structures in the study area. This work also shows the value of ASTER data as an expeditious method for geological mapping in difficult mountainous terrains such as the Frontal Cordillera, and its capabilities for recognizing lithological, alteration, and structural features. The methodology applied here can be expanded to other areas of the Frontal Cordillera and the Andes.

2. Geological framework

At ~30°30' S, the Andes are subdivided into five main morphostructural units: the Coastal Range, Principal Cordillera, Frontal Cordillera, Precordillera, and Sierras Pampeanas (Fig. 1B). The Frontal Cordillera comprises several mountain ranges in Argentina and Chile, characterized by high elevations and rugged topography. The study area covers the eastern flank of the Frontal Cordillera, including the Agua Negra International Pass, the Agua Negra, Agua Blanca, and Chita creeks, and surrounding mountain ranges (Fig. 1C). The Iglesia Valley extends to the east, separating the Frontal Cordillera from the Precordillera.

2.1. Stratigraphy

The oldest outcrops in the region correspond to Devonian rocks (Furque, 1962; Gutiérrez, 1983) and to the Upper Carboniferous-Lower Permian Agua Negra Formation (Aparicio, 1969; Polanski, 1970), exposed in the eastern sector of the study area (Fig. 2). Both units are dominated by shale and sandstone successions with very low-grade metamorphism (Cardó *et al.*, 2005; Spalletti *et al.*, 2012), and are intruded by Permian-Triassic granitoids that are part of the Colanguil Batholith (Llambías and Sato, 1990, 1995).

Towards the west, Permian-Triassic volcanic rocks crop out extensively (Fig. 2). In Argentina, these rocks are assigned to the Choiyoi Group (Llambías and Sato, 1990; Sato and Llambías, 1993). The Choiyoi Group consists of a complex set of lavas, pyroclastic rocks, and subvolcanic intrusions, mostly of intermediate to acid composition, and subordinate epiclastic rocks (Sato and Llambías, 1993; Sato *et al.*, 2015; Bastías-Mercado *et al.*, 2020). Although Choiyoi outcrops dominate an important part of the

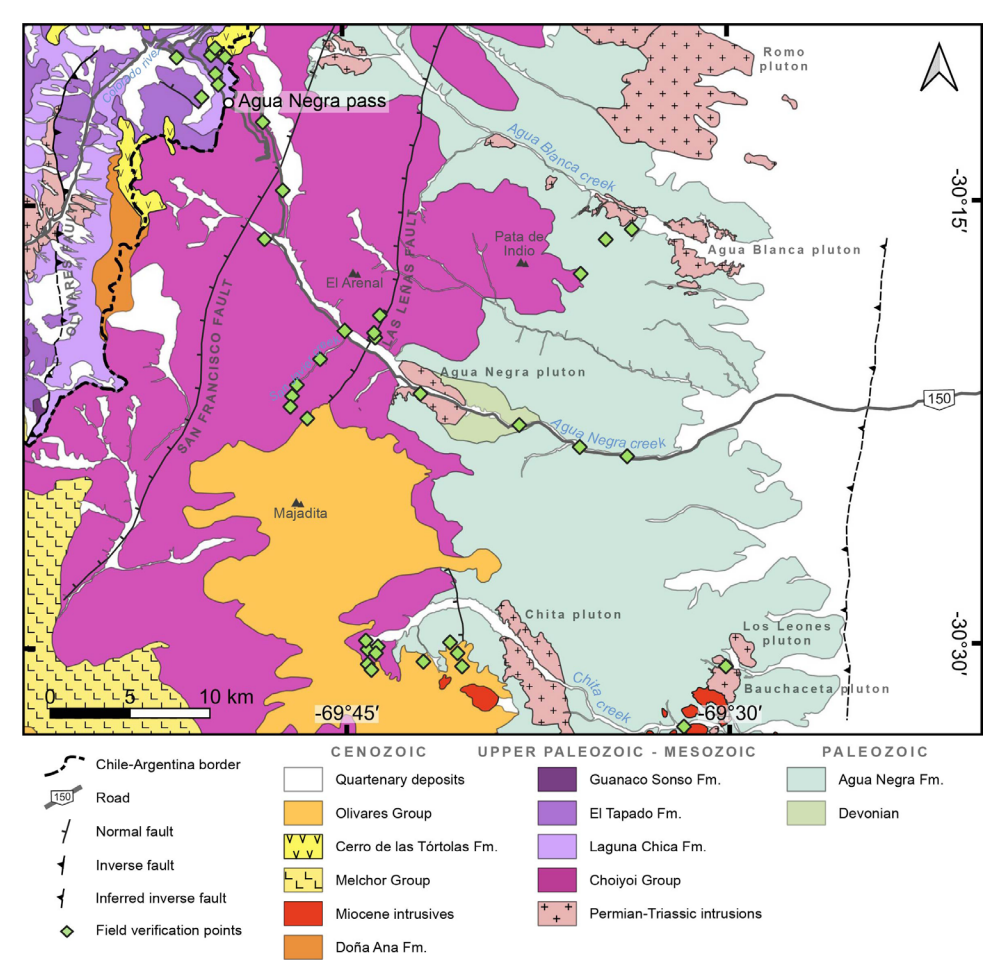


FIG. 2. Geological map of the study area. Based on and modified from Heredia *et al.* (2002), Cardó *et al.* (2005) and Velásquez *et al.* (2021). Plutons' names are based on Llambías and Sato (1990, 1995). Representative field verification points are shown as green diamonds.

study area, there is no clear consensus about its stratigraphy and distribution. Sato and Llambías (1993) defined two sections within the Choiyoi Group between 29°45' S and 30°20' S: (1) a lower section, up to 1,000 m-thick, consisting of volcanic rocks of intermediate composition composed of andesites and dacites with sedimentary lenses at the base, and (2) an upper rhyolitic section, with less aerial extent but reaching thicknesses >900 m (Sato and Llambías, 1993; Sato et al., 2015). Heredia et al. (2002) recognized three main stratigraphic units for the Choiyoi Group south of 30 °S, which exhibit an upsection change from andesitic to rhyolitic compositions. These units were defined as the Lower Choiyoi (Castaño Formation; Rodríguez Fernández et al., 1996), Middle Choiyoi (Vega de Los Machos Formation and El Palque Formation; Caballé, 1986), and Upper Choiyoi (Atutia Formation; Espina et al., 1998). According to these authors, the emplacement of these units occurred in an extensional environment, with normal faults controlling their deposition (Heredia et al., 2002; Rocher and Vallecillo, 2014; Castillo Herrera, 2021). Finally, Cardó et al. (2005) recognize three formations for the Choiyoi Group in the Castaño River region, south of the study area: the Castaño Formation, which is characterized by sedimentary and pyroclastic intercalations; the Las Chilcas Formation, dominated by andesites with subordinated basalts, dacites, scarce rhyolites and pyroclastic deposits; and the Las Pircas Formation, correlated with the El Palque Formation and composed of dacitic subvolcanic intrusions, dacitic and rhyolitic lavas, and pyroclastic deposits. The scarce age constraints available in Argentina also hinders the distinction of units within the Choiyoi Group and their correlation with Permian-Triassic volcanic units identified in other regions. Only five absolute ages were obtained in the eastern Frontal Cordillera near ~30° S: two Rb-Sr ages of 289.2±19.3 Ma and 247.6±3 Ma (Sato and Llambías, 1993), a U-Pb age of 272.8±3.4 Ma obtained next to the Agua Negra creek (Sato et al., 2015), and two ages obtained north of the study area, in the Valle del Cura region, that include an ⁴⁰Ar/³⁹Ar age of 261.0±5.4 Ma (Bissig et al., 2001) and a U-Pb age of 269.7±2.6 Ma (Jones et al., 2016). In Chile, Permian-Triassic volcanic rocks are assigned to the Laguna Chica (Middle Permian), El Tapado (Middle-Upper Permian), and Guanaco Sonso (Lower-Middle Triassic) formations through a 1:100,000-scale field mapping program and a robust geochronological database (Murillo et al., 2017; Velásquez et al., 2021).

The Upper Paleozoic-Triassic basement is unconformably covered by Cenozoic, mostly Miocene, volcanic rocks and subordinate epiclastic continental deposits (Fig. 2). This younger cover includes the Doña Ana Formation (Tillito Member, Upper Oligocene-Lower Miocene; Maksaev et al., 1984; Murillo et al., 2017), the Melchor Group (tentatively of Miocene age; Rodríguez Fernández et al., 1996; Cardó et al., 2005), the Cerro de las Tórtolas Formation (Middle Miocene; Maksaev et al., 1984; Murillo et al., 2017), and the Olivares Group (tentatively of Miocene-Pliocene age; Rodríguez Fernández et al., 1996, 1999; Heredia et al., 2002). The Doña Ana Formation consists mostly of andesitic to rhyolitic pyroclastic deposits, while the Melchor Group is characterized by andesitic pyroclastic deposits and lavas (lower part), and sedimentary rocks with volcanic clasts (upper part) (Heredia et al., 2002). The Cerro de las Tórtolas Formation and the Olivares Group are represented by andesitic to dacitic lavas and pyroclastic deposits (Cardó et al., 2005; Murillo et al., 2017; Velásquez et al., 2021). Finally, Miocene stocks and small intrusives, mostly dacitic in composition, are distributed along the easternmost margin of the Frontal Cordillera (Cardó et al., 2005; Wetten, 2005; Poma et al., 2017). Porphyry-type deposits with Cu-Mo-Au-Ag mineralization have been associated with these intrusions (Sillitoe, 1977; Burga *et al.*, 2018¹).

2.2. Structure

The current configuration of the Frontal Cordillera is the result of thick-skinned Andean deformation, mostly characterized by N-S and NNE-SSW-striking, bivergent, low- to high-angle faults that limit large basement blocks (Mpodozis and Cornejo, 1986; Moscoso and Mpodozis, 1988; Heredia et al., 2002; Martínez et al., 2015; Giambiagi et al., 2017; Velásquez et al., 2021) (Fig. 2). Previous authors have interpreted that several of these structures correspond to pre-existing normal faults, linked to the Permian-Triassic extension that characterized the Choiyoi Group emplacement (Heredia et al., 2002). Some of these faults were partially inverted during Andean compression, combined with the development of new contractional structures (Mpodozis and Ramos, 1989; Heredia et al., 2002; Martínez et al., 2015). In addition to the main structures, smaller-scale reverse and strike-slip faults are also recognized (Heredia et al., 2002; Giambiagi et al., 2017). The structural features of the Frontal Cordillera may have controlled the spatial distribution of Miocene intrusions, alteration zones, and mineral deposits, as proposed in previous works (Davidson and Mpodozis, 1991; Giambiagi et al., 2017, 2021; Burga et al., 2018; Perelló et al., 2023).

3. Methods

Satellite multispectral imagery used in this study was obtained by the Advanced Spaceborne Thermal Emission and Reflection Radiometer (ASTER) instrument, which consists of three separate instrument subsystems. Each subsystem operates in a different spectral region: visible and near-infrared (VNIR, $0.5-1.0 \,\mu\text{m}$), short-wave infrared (SWIR 1.0-2.5 $\,\mu\text{m}$), and thermal infrared (TIR, 8.0-12.0 µm). VNIR has three bands (1-3) with 15 m spatial resolution, SWIR has six bands (4-9) with 30 m spatial resolution, and TIR has five bands (10-14) with 90 m spatial resolution (Yamaguchi et al., 1998; Abrams and Hook, 2002). The different regions of the spectrum are sensitive to different rock-forming minerals: VNIR is sensitive to the presence of oxides, SWIR is sensitive to Al-OH minerals (e.g., kaolinite and muscovite), Mg-Fe-OH minerals (e.g., epidote and chlorite) and carbonates, and TIR is sensitive to minerals such as quartz and feldspar (Abrams and Hook, 1995; Rowan and Mars, 2003).

Burga, D.; Yassa, A.; Puritch, E.; Hayden, A. 2018. NI 43-101 - Technical Report and update mineral resource estimate on the Chita Vally Proyect, San Juan Province, Argentina. Minsud Resources Corp: 235 p.

For this study, we used ASTER L2 Surface Reflectance VNIR and Crosstalk Corrected SWIR data products (AST 07XT). In AST 07XT products, both the VNIR and SWIR data are generated using the bands of the corresponding ASTER L1B image, which are crosstalk and atmospherically corrected (Mars and Rowan, 2010). These products can be ordered through the NASA's Earthdata Search website (https://search.earthdata.nasa.gov/ search?q=C1299783608-LPDAAC ECS). ASTER scenes selected (Fig. 3) were acquired on February 01, 2002 (left) and March 14, 2002 (right). These two main images were supplemented with two images acquired on February 09, 2005 (top) and March 30, 2008 (bottom). ASTER images were processed in QGIS 3.14. Because in AST 07XT products reflectance values are given as integers, all bands were rescaled to values between 0 and 1 before image processing. ASTER processing consisted of: 1) RGB color composites (false color images), 2) band ratios, and 3) calculation of spectral indices. When processing included both VNIR and SWIR bands, we converted the data to a common spatial resolution through resampling. Resampling was carried out using the nearest neighbor method, in order to preserve the spectral information of the images. We chose to resample the 30 m resolution SWIR bands to the 15 m resolution VNIR bands, to benefit from the higher spatial resolution of the VNIR bands (similar to Massironi et al., 2008; Testa et al., 2018; Baid et al., 2023; Hosseini Nasab and Agah, 2023; see Supplementary Material). The obtained results were compared to published data and selected field verification sites (point locations in Figs. 1C and 2). The color composites 468 and 731, and the band ratios 4/7 3/1 4/5, resulted the best combinations due to their good correlation with previous mapping (Heredia et al., 2002; Cardó et al., 2005; Velásquez et al., 2021) and field observations, as well as their sensitivity to lithological/mineralogical changes. These three products are shown in figure 3.

After image processing and field verification, we used the free open-source Semi-Automatic Classification Plugin (SCP; Congedo, 2021) to generate a land cover classification. Developed for QGIS, SCP allows semi-automatic classification (also known as supervised classification) of ASTER images based on spectral signatures. Representative spectral signatures can be calculated from Regions

of Interest (ROIs) created with the SCP tool. ROIs are polygons that allow the user to group sets of pixels and assign them to a "class". Subsequently, a classification algorithm classifies the whole ASTER image by comparing the spectral characteristics of each pixel to the spectral characteristics of reference classes. In this study, the classification algorithm used was the Maximum Likelihood Algorithm (Richards and Jia, 2006; Congedo, 2021). The algorithm was executed multiple times, comparing the outcomes with field data, maps, and band combinations to evaluate the classification results qualitatively. After acceptable results were obtained, we used the Classification Sieve and Edit Raster tools to remove small patches from the classification and eliminate the superposition effect between ASTER scenes. Finally, in order to evaluate the accuracy of the classification, we calculated an error matrix that compares classification results with reference data (i.e., ground-truth data) (Congalton and Green, 2019). The error matrix was obtained using random points (each sample corresponding to one pixel) created with the SCP tool.

4. Results

4.1. ASTER processing: color composite and band ratios

ASTER band combination 468 (Fig. 3A) uses three SWIR bands sensitive to lithological changes and it is useful for delineating alteration zones (Di Tommaso and Rubinstein, 2007; Testa et al., 2018). In the study area, this combination highlights the location of Permian-Triassic granitoids (Romo, Agua Blanca, Agua Negra, Los Leones, Bauchaceta, and Chita plutons) in bright white to greenish colors, which contrast with Upper Paleozoic sedimentary sequences (Devonian rocks and rocks from the Agua Negra Formation) in dark colors (Fig. 3A). Miocene stocks and associated alteration zones appear in intense pink color, although some small Miocene intrusives show colors similar to the Permian-Triassic plutons. To the west, the Choiyoi Group shows a marked change from green to gray colors. This difference is highlighted in figure 3A, where "Choiyoi 1" and "Choiyoi 2" domains are distinguished.

The combination of band ratios 4/7 3/1 4/5 (Fig. 3B) is similar to the combination 4/5 4/7 3/1 used by Testa *et al.* (2018) to differentiate lithologies

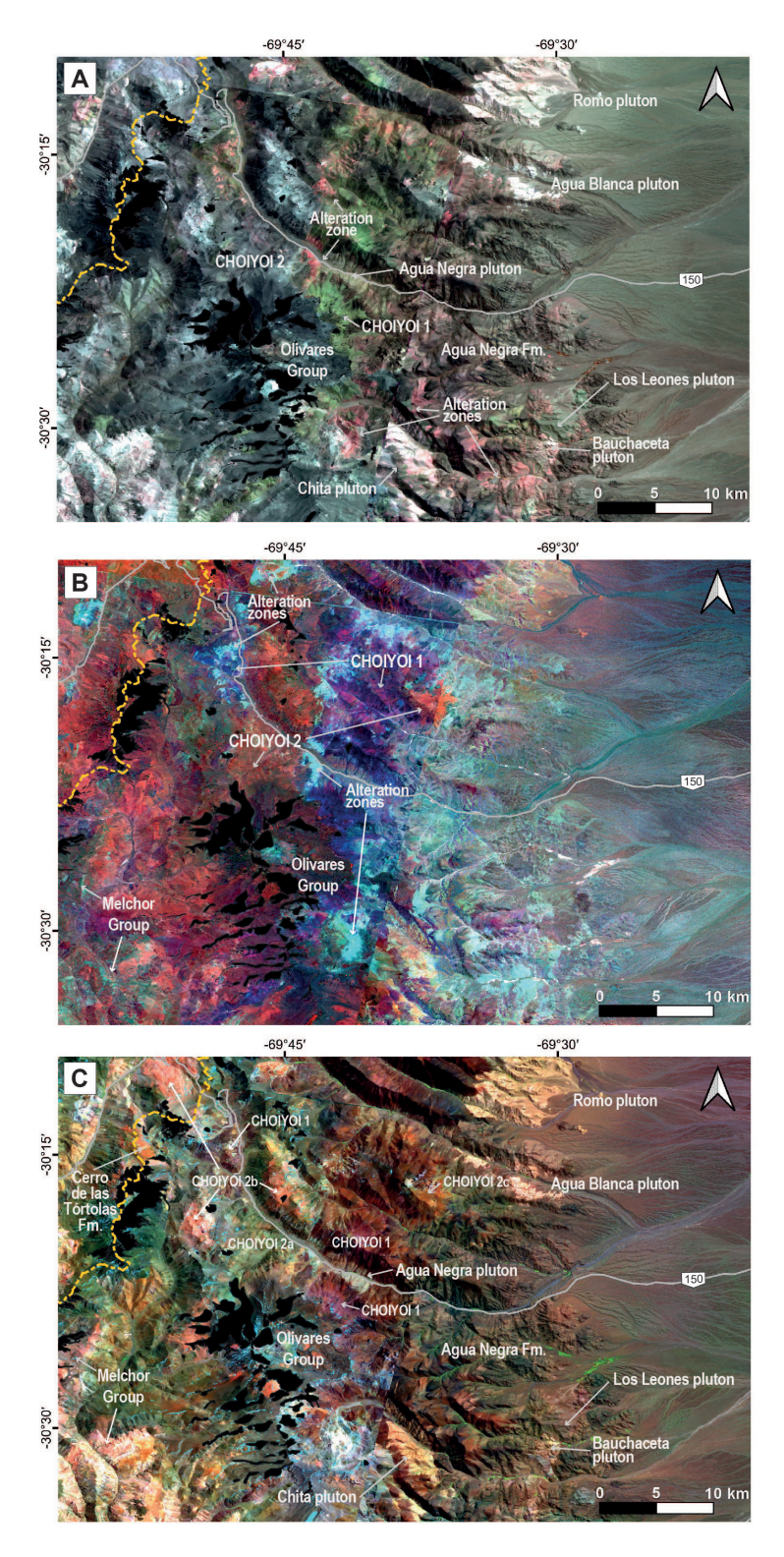


FIG. 3. ASTER processed images and their interpretation: **A.** RGB color composite 468; **B.** band ratios 4/7 3/1 4/5 as RGB color composite; **C.** RGB color composite 731.

and recognize hydrothermal alterations immediately south of the study area. While 4/5 and 4/7 ratios are aimed at detecting argillic and phyllic alterations (kaolinite has high 4/5 ratios while muscovite/illite have high 4/7 ratios), the 3/1 ratio offers contrasting spectral responses between felsic and mafic lithologies. The 4/7 3/1 4/5 combination highlights, once more, a marked change within the Choiyoi Group, which shows bright blue/violet colors to the east ("Choiyoi 1") and reddish colors to the west ("Choiyoi 2"). In addition, this band combination differentiates the Olivares Group in dark violet, while the Melchor Group is shown in green colors. Another interesting aspect shown by this combination is related to alteration zones, which are shown in bright, light blue colors. It is remarkable that parts of these alteration zones are clearly aligned with the contact between "Choiyoi 1" and "Choiyoi 2", where regional structures have also been recognized (San Francisco and Las Leñas faults in Fig. 2; Heredia et al., 2002; Cardó et al., 2005). Other alteration zones are recognized associated to Miocene intrusives along the Chita creek.

In the ASTER band combination 731 (Fig. 3C), band 7 highlights the spectral absorption of minerals such as white micas, clays, amphiboles, and epidote, while bands 1 and 3 are sensitive to Fe oxides (Massironi et al., 2008). In the study area, combination 731 discriminates Permian-Triassic plutons in bright yellowish colors. The Agua Negra Formation shows dark colors, which can change to reddish in the surroundings of large plutons. Regarding the Choiyoi Group, the eastern outcrops ("Choiyoi 1") show violet to magenta colors. Unlike combinations 468 and 4/7 3/1 4/5, western outcrops ("Choiyoi 2") can be separated into three distinguishable groups: a) green colors, b) bright reddish colors, and c) dark red colors. This could be due to a lithological difference within what was initially defined as "Choiyoi 2", here separated as "a", "b" and "c" (Fig. 3C). The Olivares Group shows different shades of gray, while the Melchor Group is distinguished in bright pink and light orange colors. Outcrops from the Cerro de las Tórtolas Formation mapped southwest of the Agua Negra pass near the Argentina-Chile border appear in a bright orange color.

4.2. Field verification

Field verification sites included several points along the Agua Negra, Chita, and San Javier creeks, Cerro Pata de Indio, and the Agua Negra pass surroundings (see Figs. 1C and 2 for locations). Devonian rocks and the Agua Negra Formation were observed in several sites along the Agua Negra and Chita creeks, where they are characterized by intercalations of sandstones and shales. Mapped Permian-Triassic plutons (Agua Negra granodiorite and Bauchaceta and Agua Blanca granites) have medium- to coarse-grained textures and are principally composed of quartz+alkali fe ldspar+plagioclase+biotite±amphibole in hand samples.

Outcrops corresponding to the "Choiyoi 1" domains in the ASTER band combinations were examined in the Agua Negra and Chita creeks. These outcrops consist mainly of altered, porphyritic volcanic rocks composed of feldspars (mostly plagioclase)±biotite±quartz±amphibole phenocrysts immersed in an aphanitic groundmass. Recognized mineral assemblages suggest andesitic to dacitic compositions. Rocks are commonly altered, which gives them greenish to black colorations. Chlorite and calcite were identified as secondary minerals. The geometry of these volcanic rocks was generally difficult to identify, although in the Chita creek tabular lavas were observed intercalated with sedimentary and pyroclastic deposits (Fig. 4A). Other deposits include levels of sandstones, shales, and limestones, as well as andesitic breccias and tuffs. In the western part of the Agua Negra creek, near the Agua Negra pass, "Choiyoi 1" is represented by greenish porphyritic rocks with large (≤5 mm) feldspar crystals. These rocks also show a significant alteration to epidote, chlorite, and calcite.

Outcrops of what was recognized as "Choiyoi 2" were observed in several places, being generally dominated by thick stacked sequences of ignimbrites with violet, gray and orange-brown tonalities. In the San Javier and Agua Negra creeks, the rocks are mostly lapilli tuffs with fiammes and feldspar (mostly plagioclase) crystaloclasts immersed in a vitric matrix (Fig. 4B). Biotite and quartz crystaloclasts were observed in a lesser proportion. Lithic clasts are also present, composed of volcanic rock fragments. Around Cerro El Arenal (Fig. 2), these ignimbrites overlie "Choiyoi 1" andesites. In Chile, near the Agua Negra pass, outcrops mapped as the Laguna Chica Formation are characterized by similar welded lapilli tuffs, corresponding to intermediate to acid ignimbrites (Velásquez et al., 2021). Lithic breccias and andesites, with minor coarse sandstones and conglomerates, were also observed in this area. The El Tapado Formation was recognized near the

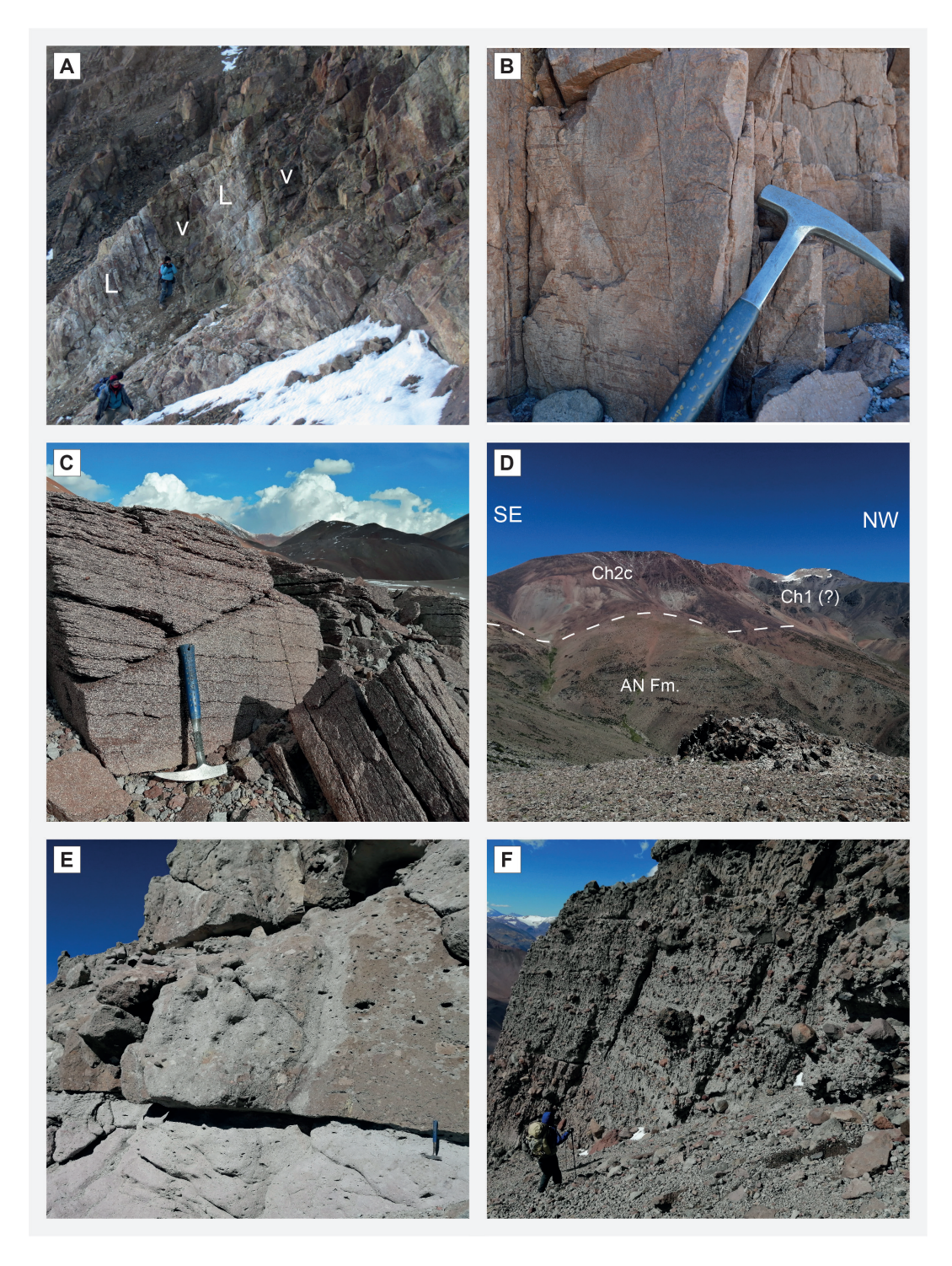


FIG. 4. A. "Choiyoi 1" outcrops in the Chita creek, consisting of interbedded porphyritic volcanic rocks (v) of andesitic to dacitic compositions, and limestones (L). B. "Choiyoi 2" ignimbrites at the San Javier creek. C. Ignimbrites from the El Tapado Formation (Choiyoi 2) near the Agua Negra pass. D. View of Cerro Pata de Indio from the NE. Around ~900 m of rhyolitic rocks (Ch2c) overlie the Agua Negra Formation (AN Fm.). Ch1: "Choiyoi 1". E. Pyroclastic breccias and lapilli tuff outcrops from the Olivares Group at the Chita creek. F. Conglomerate deposits from the Olivares Group at the San Javier creek.

Agua Negra pass as well, where it unconformably overlies the Laguna Chica Formation. Rocks of the El Tapado Formation are characterized by stratified tabular tuffs and lapilli tuffs, rich in fiammes, feldspar and biotite crystals, and volcanic rock fragments (Fig. 4C). These outcrops can be linked to dominant dacitic ignimbrites described immediately west of the study area, in the Quebrada de las Tetas (Velásquez et al., 2021). Finally, in Cerro Pata de Indio, outcrops of quartz-rich ignimbrites were recognized overlying andesitic breccias and rocks of the Agua Negra Formation (Fig. 4D). The ignimbrites consist of red to orange lapilli tuffs, with abundant quartz, feldspars (alkali feldspar and plagioclase), and fiammes. Rock fragments of andesites, rhyolites, and shales/sandstones derived from the Agua Negra Formation, are also common. Mineral mode content indicates a rhyolitic composition for these quartzrich ignimbrites.

The Olivares Group was observed in two different localities, at the headwaters of the Chita creek and in the San Javier creek. At the headwaters of the Chita creek, where it overlies the Agua Negra Formation and "Choiyoi 1" volcanic rocks, it consists of gray to light violet lapilli tuffs and tuff breccias (Fig. 4E). The rocks are rich in plagioclase+biotite±amph ibole±quartz crystaloclasts and lithic fragments, immersed in a very fine ash matrix. Lithic clasts are mostly pyroclastic and andesite fragments. In addition, subordinated volcaniclastic sandstones and conglomerates were recognized; so were small subvolcanic intrusives and dikes of andesitic to dacitic composition. In the San Javier creek, the Olivares Group rests over "Choiyoi 2" ignimbrites. Outcrops are dominated by coarse conglomerates and minor conglomeratic sandstone levels (Fig. 4F). Conglomerates are matrix- to clast-supported, presenting an ashy matrix and andesite and dacite clasts. The Cerro de las Tórtolas Formation was only observed north of the Agua Negra pass, where it is characterized by porphyritic dacites, andesites, and pyroclastic deposits. Pyroclastic deposits consist mostly of tuff breccias and lapilli tuffs rich in plagioclase and biotite crystaloclasts, as well as pumice and lithic fragments.

4.3. Supervised classification

Following ASTER color composite images and field observations, ten representative classes were

defined for the SCP supervised classification and grouped into six macroclasses (Table 1). Classes were focused on the geological units examined in the field: the Agua Negra Formation, the Permian-Triassic plutons, the Choiyoi Group, and the Olivares Group. The Melchor Group and the Doña Ana Formation were not visited in the field, while the Cerro de las Tórtolas Formation was only observed near the Agua Negra pass. Although these units were not included in the classification, their relationship with the color composite image and supervised classification analyses is discussed later. At the time of the creation of ROIs (Regions of Interest), polygons were drawn manually over relatively uniform color areas within ASTER color composites (combinations 468, 731, and 4/7 3/1 4/5) that included field observations points. In order to adjust spectral signatures and improve classification results, some unvisited areas were later included in the ROIs.

The classes defined for the SCP classification are:

- Macroclass 1: Upper Paleozoic sedimentary rocks, which include Devonian outcrops and the Agua Negra Formation. Class 1a corresponds to extensive sandstone and shale intercalations located in the easternmost sector of the Frontal Cordillera. Class 1b discriminates those outcrops affected by the intrusion of plutons, which show distinctive features in ASTER band combination 731 (Fig. 3C). The spectral signatures of both classes exhibit similar curves (Fig. 5). Therefore, and for the sake of simplicity, they are analyzed together.
- Macroclass 2: Permian-Triassic plutons, dominated by granites and granodiorites. Spectral signals of several plutons were averaged in order to obtain a representative spectral signature, which is distinguished by showing high reflectance values for most ASTER bands, particularly band 4.
- Macroclass 3: Corresponds to the "Choiyoi 1" recognized in combinations 468, 4/7 3/1 4/5, and 731. According to field observations, this class consists mainly of porphyritic volcanic rocks, which show intense propylitic alteration. Mineral assemblages of several outcrops (for example, those observed in the Chita creek and Cerro El Arenal) suggest andesitic to dacitic compositions. Subordinated pyroclastic deposits (tuffs and tuff breccias), as well as sedimentary levels of sandstones, shales and limestones, are interbedded with the volcanic rocks. Spectral

TABLE 1. SUMMARY OF THE MAIN LITHOLOGIC UNITS AND GEOLOGICAL FEATURES PRESENTED IN THIS STUDY, WHICH CORRESPOND TO THE SIX MACROCLASSES DEFINED FOR SCP CLASSIFICATION.

| Geological features and lithologic units | Description based on field observations | Distribution and spatial relationship with other units | Detection with aster products | Additional comments | | |
|--|---|--|--|--|--|--|
| Upper Paleozoic sedimentary rocks (Devonian deposits and the Agua Negra Formation) MACROCLASS 1 | Shale and sandstone successions with low-grade metamorphism. | Crops out extensively in the eastern part of the Frontal Cordillera. The Agua Negra Formation unconformably overlies the Devonian deposits. | In the combination 468 shows opaque dark colors. Clearly distinguishable from Permian-Triassic intrusives (bright white colors) and volcanic rocks (Choiyoi 1: green; Choiyoi 2: gray). In the combination 731 shows dark colors, which can change to reddish colors in the surroundings of larger intrusives. Can be difficult to differentiate from Choiyoi 1 (violet/magenta). | - | | |
| Permian-Triassic intrusions MACROCLASS 2 | Agua Negra, Bauchaceta, and Agua Blanca plutons: granites and granodiorites, with medium- to coarse-grained textures. Mainly composed of quartz+alkali feldspar+plagioclase+biotite±amphibole. | Plutons intrude the Devonian deposits and the Agua Negra Formation. | • Highlighted by 468 (bright white to greenish colors) and 731 (bright yellowish colors) band combinations. | - | | |
| Choiyoi 1 MACROCLASS 3 | Porphyritic volcanic rocks with an intense propylitic alteration. Recognized mineral assemblages (plagioclase±biotite±quartz±amphibole) suggest andesitic to dacitic compositions at the Chita creek and Cerro El Arenal. Recognized secondary minerals: chlorite+epidote+calcite. Subordinated pyroclastic deposits (tuffs and tuff breccias) and sedimentary levels of sandstones, shales and limestones. | Choiyoi 1 crops out along a NNE strip that extends across the central part of the study area (including the Chita, Agua Negra and Agua Blanca creeks), and a smaller area located southeast from the Agua Negra pass. Choiyoi 1 unconformably overlies the Agua Negra Formation. | Highlighted by 468 (green). Strong contrast with Choiyoi 2 (gray colors). In the combination 4/7 3/1 4/5 shows blue/violet colors. Notable contrast with Choiyoi 2 (reddish colors). In the combination 731 shows violet to magenta colors. It can be difficult to distinguish from the Agua Negra Formation (reddish colors in the surroundings of larger intrusives). | • Sato and Llambías (1993) include Choiyoi 1 outcrops in the "lower intermediate section". | | |

table 1 continued.

| Geological features and lithologic units | Description based on field observations | Distribution and spatial relationship with other units | Detection with aster products | Additional comments | | |
|--|--|---|---|--|--|--|
| Choiyoi 2 | Dominated by thick stacked sequences of ignimbrites, separated here in three classes: | Choiyoi 2a and Choiyoi 2b dominate the western part of the study area. | • In the combinations 468 and 4/7 3/1 4/5, Choiyoi 2 (in gray and reddish | • Sato and Llambías (1993) include Choiyoi 2a and 2b ignimbrites in the | | |
| MACROCLASS 4 | Choiyoi 2a: mostly lapilli tuffs of violet, gray and orange-brown colors, usually showing a remarkable welding and massive appearance. Rich in feldspar crystaloclasts (mostly plagioclase) and with a relatively low quartz content. Fiammes and volcanic rock fragments are present. Choiyoi 2b: stratified outcrops of violet and gray tabular tuffs and lapilli tuffs. Rich in feldspar crystaloclasts (mostly plagioclase) and with a relatively low quartz content. Fiammes and volcanic rock fragments are present. Choiyoi 2c: red to orange lapilli tuffs, with abundant quartz, feldspars (alkali feldspar and plagioclase) and fiammes. Rock fragments (volcanic rocks and shales/sandstones derived from the Agua Negra Formation) are common. | In Cerro El Arenal, Choiyoi 2a ignimbrites overlie Choiyoi 1 andesites/dacites. | colors, respectively) shows a marked contrast with Choiyoi 1 (green and blue/violet, respectively). • The combination 731 is the only ASTER band combination that highlights the differences between the three Choiyoi 2 classes: Choiyoi 2a (green), Choiyoi 2b (bright red) and Choiyoi 2c (dark red). | "lower intermediate section". According to Sato and Llambías (1993), Choiyoi 2c ignimbrites in Cerro Pata de Indio represent the "upper rhyolitic section". Rocks mapped as Laguna Chica Formation in Chile are generally classified as Choiyoi 2a. Our results, together with the available age constraints, support the correlation between Choiyoi 2a outcrops in Argentina and the Laguna Chica Formation. Rocks mapped as El Tapado Formation in Chile are generally classified as Choiyoi 2b. Our results, together with the described spatial relationships, suggest a tentative correlation between the El Tapado Formation and Choiyoi 2b outcrops in Argentina. | | |

table 1 continued.

| Geological features and lithologic units | Description based on field observations | Distribution and spatial relationship with other units | Detection with aster products | Additional comments | | |
|--|--|---|--|---|--|--|
| Olivares Group | Dominantly pyroclastic deposits: composed of plagioclase+biotite± | The Olivares Group outcrops mostly around Cerro Majadita. It overlies the | • Clearly differentiated by combination 731 (gray). | SCPclassification is able to discriminate between the dominantly pyroclastic | | |
| MACROCLASS 5 | amphibole±quartz crystaloclasts and lithic fragments (pyroclastic rocks and andesites), immersed in a very fine ash matrix. Subordinated volcaniclastic sandstones and conglomerates, and andesitic/dacitic dykes. Dominantly epiclastic deposits: coarse conglomerates and minor conglomeratic sandstone levels. Conglomerates are matrix- to clast-supported and are composed of andesite and dacite clasts in an ash matrix. | Agua Negra Formation and Choiyoi 1 and Choiyoi 2 volcanic rocks. Dominantly pyroclastic deposits are found in the eastern flank of Cerro Majadita and in the headwaters of the Chita creek, while outcrops located to the west are dominated by epiclastic deposits. | Recognizable in 468 (dark gray) and 4/7 3/1 4/5 (dark violet/blue) combinations. None of the ASTER band combinations used in this study is capable of distinguishing between dominantly pyroclastic and dominantly epiclastic deposits within the Olivares Group. | and the dominantly epiclastic deposits within the Olivares Group. Epiclastic deposits are probably more abundant than previously thought. | | |
| Alteration zones MACROCLASS 6 | *Interpreted as argillic-phyllic hydrothermal alteration zones based on ASTER band combination results and obtained spectral signatures. | (Chita creek) and major faults (Las | • Highlighted by 468 (pink) and 4/7 3/1 4/5 (bright, light blue) combinations. | • Using the alteration zones, the Las Leñas fault was outlined in the geological map. This fault puts in contact the altered porphyritic rocks from Choiyoi 1 and the ignimbrites from Choiyoi 2a. The Las Leñas and San Francisco faults were previously recognized as main structures in the study area by Heredia et al. (2002). | | |

The table includes a description of each macroclass (based on field observations), their distribution and spatial relationship with other units (based on field observations and SCP results), and how these features are detected using ASTER products (band combinations). The last column has additional comments, such as mentions of the recognized lithological units in the revised literature.

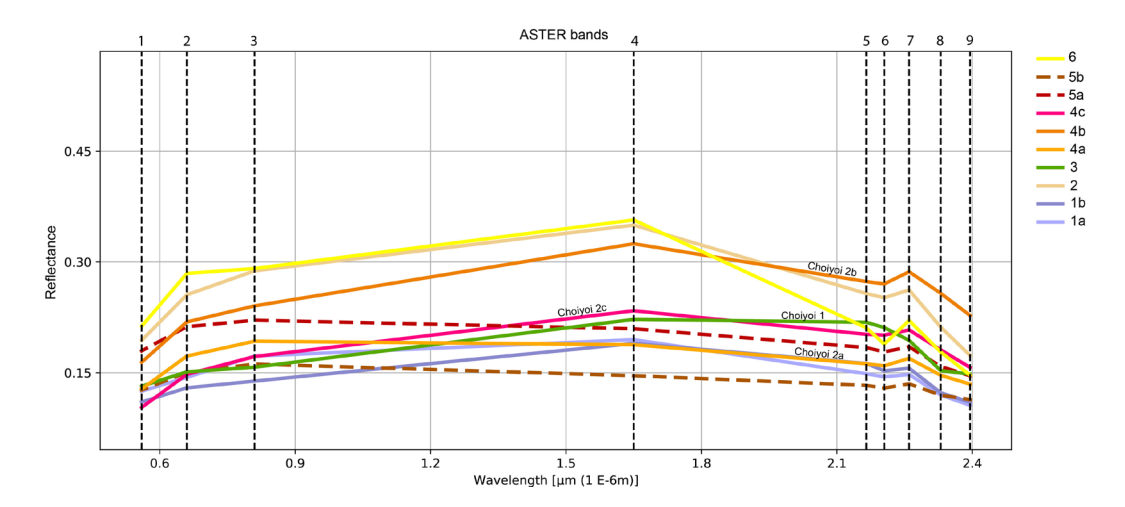


FIG. 5. Representative classes' spectral signatures, calculated with SCP. Classes: 1a: Upper Paleozoic sedimentary rocks; 1b: Upper Paleozoic sedimentary rocks affected by the intrusion of plutons; 2: Permian-Triassic intrusions; 3: Porphyritic rocks with propylitic alteration and pyroclastic/sedimentary intercalations (Choiyoi 1); 4a: Quartz-poor massive ignimbrites (Choiyoi 2a); 4b: Quartz-poor layered ignimbrites (Choiyoi 2b); 4c: Quartz-rich ignimbrites (Choiyoi 2c); 5a: Pyroclastic deposits (Olivares Group); 5b: Epiclastic deposits (Olivares Group); 6: Alteration zones.

signature for class 3 shows low reflectance values for band 8 (Fig. 5), which can be related with absorption of mineral species such as chlorite, epidote, amphibole and/or carbonates (Mars and Rowan, 2006; Di Tommaso and Rubinstein, 2007). In this case, reflectance values can be correlated with the strong alteration described in field observations.

Macroclass 4: corresponds to the "Choiyoi 2", being largely dominated by thick sequences of ignimbrites. Based on the results from band combination 731, three classes were defined. In this color composite image, ignimbrites rich in feldspars and with a relatively low quartz content exhibit green and bright reddish colors. This led to the creation of classes 4a and 4b, respectively. Both spectral signature curves show a similar shape but differ in reflectance values (Fig. 5). In field observations, ignimbrites from both classes appear to have similar compositions. However, class 4a outcrops typically exhibit more intense welding and a massive appearance, while class 4b outcrops display stacked, well-defined tabular levels. The third class, 4c, represented by dark red colors in combination 731, corresponds to quartz-rich ignimbrites observed in Cerro Pata de Indio. The spectral signature curve for 4c

- differs from 4a and 4b by exhibiting lower values in bands 1 to 3, while also displaying peaks in bands 4 and 7 (Fig. 5).
- Macroclass 5: is constituted by the Olivares Group deposits. In the field, it was possible to differentiate two main lithologies: pyroclastic deposits of andesitic to dacitic composition, recognized near the headwaters of the Chita creek, and conglomerates with andesite and dacite clasts, recognized in the San Javier creek. Although these lithological differences are not as evident in the color composite images, two separate classes, 5a and 5b, were created for the Olivares Group following field observations. This resulted in two spectral curves of a similar shape, but clearly distinguishable from each other in their reflectance values (Fig. 4).
- Macroclass 6: includes large hydrothermal alteration zones recognized in composite color images. These zones are highlighted in band combinations 468 and 4/7 3/1 4/5 in pink and light blue colors, respectively. These colors respond to argillic-phyllic alterations (Testa *et al.*, 2018). The spectral signature shows an important absorption in band 6, typically caused by phyllic alteration, rich in muscovite and illite (Mars and Rowan, 2006; Testa *et al.*, 2018).

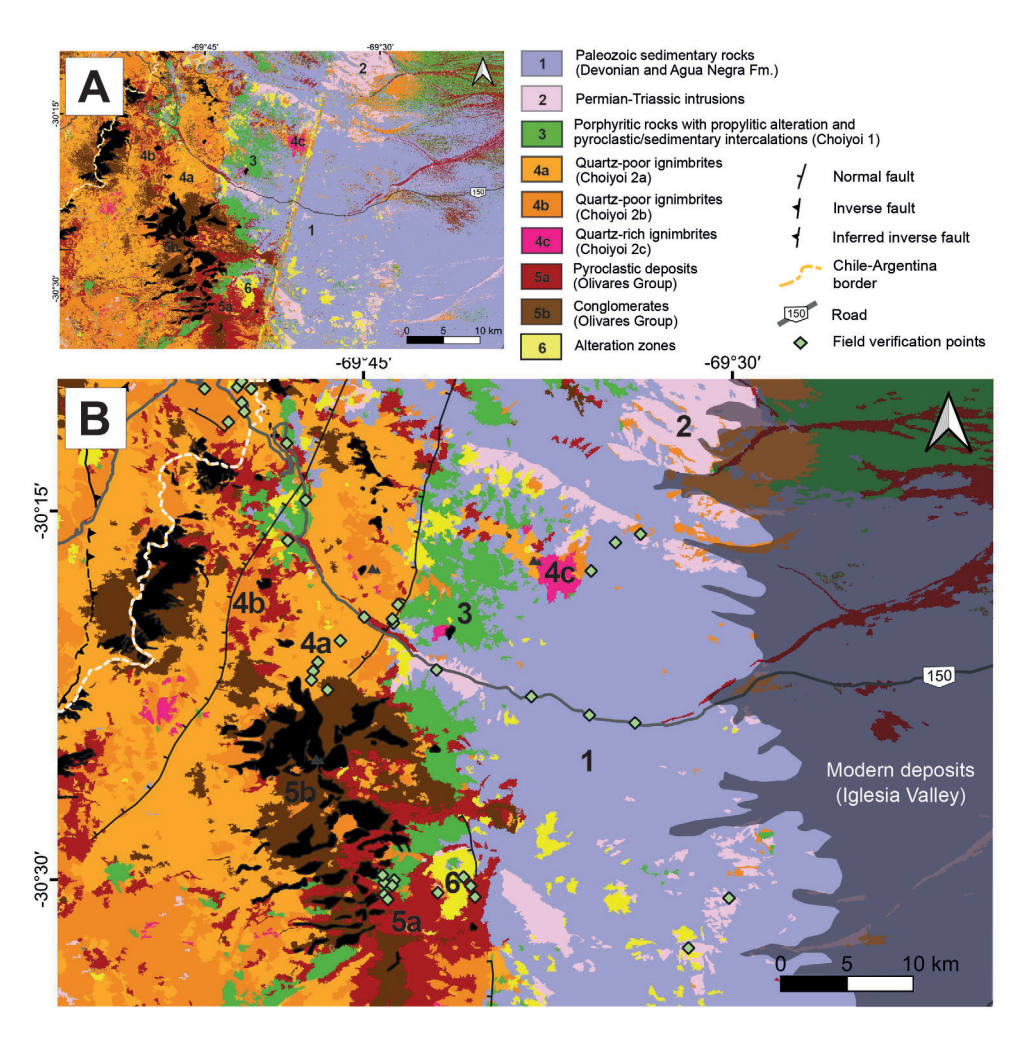


FIG. 6. Supervised classification results, obtained with SCP. Note that classes 1a and 1b from Fig. 5 were merged, grouping all Upper Paleozoic sedimentary rocks. A. Raw results; note the patchy appearance of the classes and the NE-trending yellow line corresponding to the limit between two ASTER scenes. B. Smoothed results after using the Classification Sieve and Edit Raster tools. Field verification points and mapped faults are represented.

Figure 6 shows the results of the SCP classification, before and after performing Classification Sieve and Edit Raster corrections (Fig. 6A and B respectively). The classification shows overall satisfactory results. Upper Paleozoic sedimentary rocks and Permian-Triassic plutons are well differentiated from the other lithologies. Regarding volcanic units (Choiyoi Group and Olivares Group), the SCP classification is capable of discriminating between classes, although results are more scattered, classes' boundaries are more complex, and some inconsistencies are recognized, *e.g.*, patches in the northwest of the study area that are classified as Olivares Group rocks that likely correspond to Choiyoi Group volcanics.

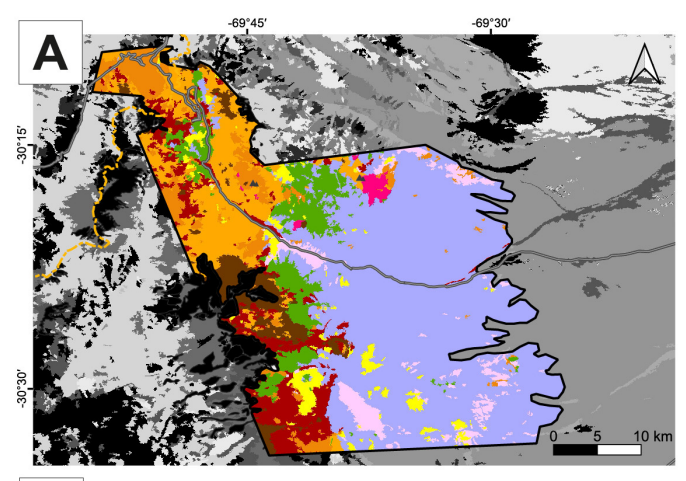
Results show that class 3, corresponding to Choiyoi 1, is distributed in two NNE-oriented strips (Fig. 6). One extends across the central part of the study area, passing through the Agua Blanca, Agua Negra, and Chita creeks. The other covers a smaller area and is located east and southeast of the Agua Negra pass. Both strips overlap with major faults (San Francisco and Las Leñas; see Fig. 2). Choiyoi 2 dominates the western part of the study area. According to the SCP classification, most outcrops in Argentina correspond to class 4a ignimbrites, with smaller outcrops of class 4b ignimbrites on top of them. In Chile, outcrops mapped as the Laguna Chica Formation are usually classified as 4a ignimbrites,

while the El Tapado Formation corresponds with 4b ignimbrites. Class 4c, representing quartz-rich ignimbrites, was only recognized in two small areas, one in Cerro Pata de Indio and the other west of the study area, near the Argentina-Chile border.

The classification was also able to discriminate between the dominantly pyroclastic (class 5a) and dominantly epiclastic (class 5b) deposits from the Olivares Group. According to the SCP classification, Olivares Group outcrops in the eastern flank of Cerro Majadita and in the headwaters of the Chita creek consist mostly of pyroclastic deposits, while those located to the west are dominated by epiclastic deposits. Regarding class 6, SCP classification delineates argillic-phyllic alteration zones related

to Miocene intrusives (distributed along the Chita creek) and major faults. Finally, the Doña Ana Formation, the Melchor Group, and the Cerro de las Tórtolas Formation, which were not included in the representative classes, were classified as classes 4b, 5a, and 5b by SCP.

In order to evaluate the reliability of the classification results, 500 points (pixels) were generated in a random stratified sampling. Stratified sampling implies that the ten reference classes were sampled proportionately to the area they represented in the SCP classification (Fig. 7). Samples were collected from a region of reference (*i.e.*, of reliable lithological information) defined within the study area and supported by field verification sites, previous



| В | Sample stratification | | | | | | | |
|---|-----------------------|---------------------|--------------------|-----------------------|------|--|--|--|
| | Class | Area [%] | Equal distribution | Weighted distribution | Mean | | | |
| | 1a + 1b | 49.91 | 100 | 257.48 | 178 | | | |
| | 2 | 5.11 | 50 | 22.46 | 36 | | | |
| | 3 | 7.79 | 50 | 37.83 | 44 | | | |
| | 4a | 4a 13.29 4b 6.08 | | 61.43 | 58 | | | |
| | 4b | | | 33.50 | 42 | | | |
| | 4c | 0.69 | 50 | 3.83 | 27 | | | |
| | 5a | 8.61 | 50 | 43.45 | 46 | | | |
| | 5b | 5b 4.62 | | 23.57 | 36 | | | |
| | 6 | 3.90 | 50 | 16.45 | 33 | | | |
| F | TOTAL OF SA | MPLES (N) | | | 500 | | | |

Area [%] = mapped area proportion of a class Equal distribution = N / number of classes = 500/10 = 50Weighted distribution = Area * NMean = (N / number of classes + Area * N) / 2

FIG. 7. Sample design for the Accuracy Assessment. A. Region of reference, from where random pixels were collected for the calculation of the error matrix. **B.** Stratified sampling calculation. The number of samples for a determined class is defined considering the mean value between equal distribution (N/number of classes) and weighted distribution (N*area).

geological mapping (Velásquez et al., 2021) and high-resolution satellite images (ESRI and Google Earth). The error matrix (Congalton and Green, 2019), and the area-based error matrix (Olofsson et al., 2014) and related accuracy parameters were calculated using the SCP tool (Table 2). Results show good reliability with an overall accuracy of 81.25%. On the other hand, inconsistencies observed in the classification are likely related to: 1) lithological variability within units, and 2) the fact that classes, especially those related to volcanic units, show similarities in their spectral signatures (Fig. 5), probably related to similarities in their lithologies and composition. This last issue is highlighted in table 2, where the lowest pairs of accuracy measures (producer's accuracy and user's accuracy) correspond to classes 4a, 4b, and 5a (Choiyoi and Olivares volcanic rocks). Permian-Triassic granitoids (class 2) also show relatively low accuracy values. Finally, it has to be taken into consideration that talus and alluvial deposits that cover rock outcrops affect the classification process as well.

5. Discussion

5.1. Interpretation of ASTER imagery processing and geological framework of the eastern flank of the Frontal Cordillera

ASTER color composite and band ratios, combined with field verifications, provide an effective method for differentiating geological features and lithologic units in the study area. The Upper Paleozoic sedimentary rocks and Permian-Triassic intrusives are clearly distinguishable using ASTER band combinations, especially 468 and 731 color composites. On the other hand, ASTER imagery was tested to discriminate different lithological units from Permian-Triassic and Cenozoic volcanic rocks in the central and western part of the study area. The lithological similarities of these units (mostly composed of lavas and pyroclastic rocks of intermediate to acid composition, with subordinated sedimentary levels), and the difficulties to access to fresh outcrops, made their recognition and mapping a challenging task, especially in Argentina, where detailed field studies and geochronology data are scarce. We have described how ASTER image processing is able to capture lithological differences through 468, 731, and 4/7 3/1 4/5 color composite images. The 731 is

the most comprehensive combination and it clearly distinguishes the Olivares and Melchor Groups from the Choiyoi Group. Furthermore, it is the only band combination that recognizes lithological differences within the western outcrops of Choiyoi Group.

ASTER 468 and 4/7 3/1 4/5 combinations allow to discriminate two main groups of rocks within the Choiyoi Group, here called "Choiyoi 1" and "Choiyoi 2" (Fig. 3A and B). According to field observations, Choiyoi 1 consists mainly of porphyritic rocks usually strongly alterated to epidote, chlorite, and calcite. Observed mineral assemblages in several of these rocks (as those recognized in the Chita creek and Cerro El Arenal) suggests andesitic to dacitic compositions. Subordinated pyroclastic, epiclastic and limestone levels are intercalated with these volcanic rocks. Choiyoi 2 is composed mainly of ignimbrites and overlies Choiyoi 1 rocks. Field observations show that a large number of outcrops are dominated by stacked levels of ignimbrites rich in plagioclase and with a relatively low quartz content (Choiyoi 2a and Choiyoi 2b). These deposits extend along the western part of the study area (Fig. 3C). Finally, quartz-rich ignimbrites (Choiyoi 2c) are restricted to small areas, as in Cerro Pata de Indio (Fig. 3C).

Regarding younger volcanic units, the Olivares Group is clearly distinguishable in 468, 731, and 4/7 3/1 4/5 ASTER combinations. Field observations showed the presence of, at least, two deposit types within the Olivares Group: one is dominantly pyroclastic and the other is dominantly epiclastic. The Doña Ana and the Cerro de las Tórtolas formations were mapped in the Argentina-Chile border (Fig. 2; Velásquez et al., 2021), and the Melchor Group was recognized in the southwest of the study area (Fig. 2; Heredia et al., 2002). ASTER imagery processing results do not show distinctive features to recognize the Doña Ana Formation; this could be related to their limited outcrops in the study area in addition to the lithological complexities mentioned in the previous section. Conversely, the Cerro de las Tórtolas Formation outcrops are partly recognized in ASTER band combination 731. The Melchor Group is clearly distinguishable in this combination as well (Fig. 3C).

In addition to the recognition of lithologic units, ASTER band combinations can also be used to outline major structures in the study area. The 4/7 3/1 4/5 combination highlights argillic-phyllic alteration zones, some of which are clearly aligned, suggesting

TABLE 2. ACCURACY ASSESSMENT RESULTS FOR SCP CLASSIFICATION USING THE MAXIMUM LIKELIHOOD ALGORITHM.

A) Error matrix (pixel count)

| Reference dat | I | Re | fei | ren | ce | d | at | t٤ | 1 |
|---------------|---|----|-----|-----|----|---|----|----|---|
|---------------|---|----|-----|-----|----|---|----|----|---|

| | | 1 | 2 | 3 | 4a | 4b | 4c | 5a | 5b | 6 | Total |
|----------------|-------|-----|----|----|----|----|----|----|----|----|-------|
| | 1 | 166 | 3 | 7 | 0 | 0 | 0 | 2 | 0 | 0 | 178 |
| | 2 | 16 | 19 | 1 | 0 | 0 | 0 | 0 | 0 | 0 | 36 |
| | 3 | 7 | 0 | 37 | 0 | 0 | 0 | 0 | 0 | 0 | 44 |
| on | 4a | 0 | 0 | 6 | 42 | 6 | 0 | 2 | 2 | 0 | 58 |
| Classification | 4b | 3 | 0 | 5 | 4 | 26 | 0 | 4 | 0 | 0 | 42 |
| assif | 4c | 2 | 0 | 4 | 1 | 2 | 18 | 0 | 0 | 0 | 27 |
| Ü | 5a | 5 | 0 | 6 | 10 | 2 | 0 | 23 | 0 | 0 | 46 |
| | 5b | 2 | 0 | 0 | 8 | 1 | 0 | 1 | 24 | 0 | 36 |
| | 6 | 7 | 0 | 0 | 0 | 0 | 0 | 0 | 0 | 26 | 33 |
| | Total | 208 | 22 | 66 | 65 | 37 | 18 | 32 | 26 | 26 | 500 |

B) Area-based error matrix

Reference data

| | | 1 | 2 | 3 | 4a | 4b | 4c | 5a | 5b | 6 | Area |
|----------------|---------|-----------|----------|-----------|-----------|----------|---------|----------|----------|----------|------------|
| | 1 | 0.489 | 0.008 | 0.013 | 0.000 | 0.000 | 0.000 | 0.005 | 0.000 | 0.000 | 565901339 |
| | 2 | 0.020 | 0.024 | 0.001 | 0.000 | 0.000 | 0.000 | 0.000 | 0.000 | 0.000 | 49363426 |
| | 3 | 0.012 | 0.000 | 0.064 | 0.000 | 0.000 | 0.000 | 0.000 | 0.000 | 0.000 | 83132777 |
| | 4a | 0.000 | 0.000 | 0.013 | 0.089 | 0.013 | 0.000 | 0.004 | 0.004 | 0.000 | 135007653 |
| Classification | 4b | 0.005 | 0.000 | 0.008 | 0.006 | 0.042 | 0.000 | 0.006 | 0.000 | 0.000 | 73636426 |
| sifica | 4c | 0.001 | 0.000 | 0.001 | 0.000 | 0.001 | 0.005 | 0.000 | 0.000 | 0.000 | 8417025 |
| lass | 5a | 0.009 | 0.000 | 0.011 | 0.019 | 0.004 | 0.000 | 0.043 | 0.000 | 0.000 | 95488652 |
| | 5b | 0.003 | 0.000 | 0.000 | 0.011 | 0.001 | 0.000 | 0.001 | 0.031 | 0.000 | 51799276 |
| | 6 | 0.007 | 0.000 | 0.000 | 0.000 | 0.000 | 0.000 | 0.000 | 0.000 | 0.026 | 36159075 |
| | Total | 0.546 | 0.032 | 0.111 | 0.125 | 0.060 | 0.005 | 0.060 | 0.035 | 0.026 | 1098905653 |
| | Area | 599686815 | 35007614 | 121689271 | 137687135 | 65805907 | 5611350 | 66233632 | 38694961 | 28488969 | 1098905653 |
| | PA*[%] | 89.65 | 74.42 | 57.45 | 71.00 | 69.27 | 100.00 | 72.08 | 87.97 | 100.00 | |
| | UA**[%] | 95.19 | 52.78 | 84.09 | 72.41 | 61.90 | 66.67 | 50.00 | 65.71 | 78.79 | |
| | | | | | | | | | | | |

^{*}PA: producer's accuracy (indicates the proportion of the area of reference class j that is classified as class j, *i.e.*, indicates how many times a land cover type on the ground was identified as that land cover type on the classification).

a structural control in their location. Specifically, two NNE-trending alteration zones can be related to two major structures recognized in previous works (Heredia *et al.*, 2002; Cardó *et al.*, 2005),

corresponding to the Las Leñas and San Francisco faults (Figs. 2 and 3B). These faults would put in contact the altered porphyritic rocks from Choiyoi 1 and the ignimbrites from Choiyoi 2 (Fig. 3B).

^{**}UA: user's accuracy (indicates the proportion of the area classified as class i that has reference class i, *i.e.*, indicates how many times a land cover type on the classification is that land cover type on the ground).

Overall accuracy [%]=81.25

A. Error matrix calculated according to pixel count (Congalton and Green, 2019).

B. Area-based error matrix. Accuracy statistics calculated according to the area-based error matrix (Olofsson et al., 2014; Congedo, 2021).

ASTER imagery and field observations were used to carry out a supervised classification using the Semi-Automatic Classification Plugin (SCP). With an overall accuracy above 80%, this methodology represents a powerful tool to understand the distribution of the recognized lithological units. According to SCP classification results, outcrops of the Choiyoi Group in the study area (Fig. 6) would be mostly dominated by the stacked levels of relative quartz-poor ignimbrites that belong to Choiyoi 2a and Choiyoi 2b. Choiyoi 1 outcrops are restricted along two NE-striking strips. A small sector classified as Choiyoi 2c near the Argentina-Chile border would be the only outcrop dominated by quartz-rich ignimbrites besides Cerro Pata de Indio. SCP classification is also able to differentiate between the two lithological associations recognized within the Olivares Group, revealing their distribution around Cerro Majadita and at the headwaters of the Chita and San Javier creeks (Fig. 6). Previous studies (Charchaflié, 1994; Vitaller, 1994) have described the Olivares Group as a unit composed mostly by andesitic lavas, pyroclastic deposits and andesitic/ dacitic subvolcanic intrusions, coincident to what was seen in the Chita creek. SCP classification also suggests that epiclastic deposits would be more abundant than previously thought. On the other hand, the classification algorithm was capable of broadly differentiating both the Doña Ana and Cerro de las Tórtolas formations, classifying them as 4b, 5a, and 5b classes (Fig. 6); however, outcrop limits are not clear so the classification results do not seem to be useful for the recognition of these units. In contrast, results seem to reflect well the distribution of the Melchor Group, classified as 4b and 5a classes (Fig. 6). It is possible that with field recognition, ASTER imagery interpretation and supervised classification of these units can be improved.

Table 1 summarizes the main lithologic units and geological features examined in this work, as well as results obtained from ASTER data and the SCP classification. Overall, ASTER imagery processing and the SCP represent accessible and cost-effective tools to improve geological mapping in the study area. The methodology applied in this contribution can also be useful for mapping in other regions with difficult access and similar volcanosedimentary lithologies. Depending on the geologic context and outcrop quality, different band ratios

and combinations should be tested. ROIs can then be defined for SCP classification, shown to be an effective tool for geological mapping.

5.2. The Choiyoi Group: lithological units and correlations with Permian-Triassic formations recognized in Chile

Different authors have recognized units within the Choiyoi Group in the Frontal Cordillera at ~30° S (see section 2.1). Traditionally, the Choiyoi Group was divided into two sections: a lower section of intermediate compositions, with thin sedimentary lenses intermittently present at the base, and an upper section of acid compositions (Sato and Llambías, 1993; Sato *et al.*, 2015). Subsequently, other studies proposed the division of the Choiyoi Group into different lithostratigraphic units (Rodríguez Fernández *et al.*, 1996; Heredia *et al.*, 2002; Cardó *et al.*, 2005).

Our results support the recognition of at least three different units within the Choiyoi Group (Table 1). According to our interpretations, the basal part of the Choiyoi Group, defined here as Choiyoi 1, consist of porphyritic rocks with intense propylitic alteration, commonly intercalated with pyroclastic and sedimentary levels. The mineral assemblages observed in the field suggest andesitic to dacitic compositions for many of these rocks. These results agree with previous descriptions (the "lower section" from Sato and Llambías, 1993; the Castaño Formation, Rodríguez Fernández et al., 1996; Heredia et al., 2002; Cardó et al., 2005; the San Ignacio Formation (?), Busquets et al., 2013). This unit is followed by the stacked, relatively quartz-poor ignimbrites levels from Choiyoi 2a and 2b. According to Sato and Llambías (1993), these ignimbrites belong to the lower intermediate Choiyoi section. The quartz-rich ignimbrites defined here as Choiyoi 2c represent the uppermost unit. These rocks correspond to the upper Choiyoi section described by Sato and Llambías (1993) in Cerro Pata de Indio.

Tentative correlations between the Choiyoi Group and the Permian-Triassic units defined in Chile have been made by previous authors (Castillo Herrera, 2021; Velásquez et al., 2021). Our results show that these correlations can be supported and enhanced by ASTER image processing and SCP classification. The Laguna Chica Formation, assigned to the Middle Permian according to U-Pb ages (~275-264 Ma), was correlated with the lower

section of the Choiyoi Group (Jones et al., 2016; Salazar and Coloma, 2016; Velásquez et al., 2021). The correlation is based on a 272.8±3.4 Ma U-Pb age obtained in the Agua Negra creek (Sato et al., 2015). Our supervised classification results support this finding: the Maximum Likelihood Algorithm classifies the outcrops of Choiyoi Group around the Agua Negra creek as Choiyoi 2a, and the same occurs for most of the Laguna Chica Formation outcrops (see Figs. 2 and 6). The El Tapado Formation, assigned to the Middle-Upper Permian according to U-Pb ages (~263-256 Ma), was correlated with the upper section of the Choiyoi Group based on its stratigraphic position and lithology (Velásquez et al., 2021). Our results suggest lithological similarities between the El Tapado Formation and Choiyoi 2b ignimbrites (Figs. 3C and 6). Also, interpretation of ASTER imagery shows that Choiyoi 2b overlies Choiyoi 2a, as well as the El Tapado Formation overlies the Laguna Chica Formation. These observations point to a possible correlation between the El Tapado Formation and Choiyoi 2b ignimbrites. Instead, our results do not show a clear relation between the El Tapado Formation and the rhyolitic ignimbrites from uppermost Choiyoi 2c, located around Cerro Pata de Indio. Finally, the strongly altered porphyritic volcanic rocks from Choiyoi 1 are not identified in the Chilean side of the study area, neither in ASTER composite images nor on SCP classification results.

Although more petrological and geochronological studies are needed to properly characterize the Choiyoi Group and sustain its correlation with the Permian-Triassic units described in Chile, our results provide new significant information, corroborated by field observations and the available geochronological data, that are helpful to understand the main features and distribution of the Choiyoi Group units. Thus, ASTER processing can significantly contribute to the Permian-Triassic volcanic stratigraphy in this sector of the Frontal Cordillera, and it can potentially be extended to other sectors allowing regional correlations of the Permian-Triassic units.

6. Conclusions

The eastern flank of the Frontal Cordillera at $\sim 30^{\circ}30^{\circ}$ S is a remote, poorly studied area. In this work, we used ASTER data, coupled with field observations, to clarify the geological framework and

recognize first-order lithological units. We performed a supervised classification using the Maximum Likelihood Algorithm and defined representative classes based on processed ASTER imagery and field observations. ASTER imagery was effective in discriminating lithologies through color composite images made with 468, 731, and 4/7 3/1 4/5 band combinations. The 731 band combination was the most effective at recognizing and distinguishing between different Permian-Triassic and Cenozoic units. The SCP supervised classification produced good results, with an overall accuracy of ~81%. Although defined classes, particularly those related to volcanic units, may show complex boundaries or classification inconsistencies, SCP remains a robust tool for visualizing the distribution of recognized units in the study area.

Our main findings can be summarized as follows:

- We recognize, at least, three units within the Choiyoi Group. The basal unit is represented by porphyritic volcanic rocks and subordinated sedimentary and pyroclastic levels, normally showing a strong propylitic alteration. The middle unit is dominated by stacked levels of ignimbrites with relatively low quartz content. The upper unit was recognized in Cerro Pata de Indio and consists of quartz-rich rhyolitic ignimbrites. Tentative correlations with the Laguna Chica and El Tapado formations, mapped in Chile, are done based on ASTER data and SCP classification results.
- According to the SCP classification and field observations, the Olivares Group comprises at least two types of deposits. One is dominantly pyroclastic and is exposed in the eastern flank of Cerro Majadita and at the headwaters of the Chita creek. The other is dominantly epiclastic and is exposed in the western flank of Cerro Majadita and at the headwaters of the San Javier creek.
- ASTER data outlines major structures in the study area, recognized through alteration zones highlighted in color composite images. The San Francisco and Las Leñas faults would affect the basal and middle units recognized in the Choiyoi Group.

Acknowledgments

This work was supported by CONICET (PICT 2016-0269 and PIP 2021-1220200101409CO), the National University of Cuyo (SIIP 2022-2024 M052-T1), and the US NSF (EAR-1952791). We acknowledge S.J. Schlamelcher

Tejada for his assistance in the field, as well as the comments of A. Martínez and two anonymous reviewers that helped us to improve this work.

References

- Abrams, M.; Hook, S.J. 1995. Simulated Aster Data for Geologic Studies. IEEE Transactions on Geoscience and Remote Sensing 33 (3): 692-699.
- Abrams, M.; Hook, S. 2002. ASTER User Handbook. Jet Propulsion Laboratory/California Institute of Technology: 135 p. Pasadena.
- Abrams, M.; Yamaguchi, Y. 2019. Twenty years of ASTER contributions to lithologic mapping and mineral exploration. Remote Sensing 11 (11): 1-28.
- Aparicio, E.P. 1969. Contribución al conocimiento de la edad de los sedimentos del Arroyo Agua Negra, Departamento Iglesia, San Juan. Revista de la Asociación Geológica Argentina 24 (4): 351-356.
- Baid, S.; Tabit, A.; Algouti, A.; Algouti, A.; Nafouri, I.; Souddi, S.; Aboulfaraj, A.; Ezzahzi, S.; Elghouat, A. 2023. Lithological discrimination and mineralogical mapping using Landsat-8 OLI and ASTER remote sensing data: Igoudrane region, jbel saghro, Anti Atlas, Morocco. Heliyon 9 (7): e17363.
- Bastías-Mercado, F.; González, J.; Oliveros, V. 2020. Volumetric and compositional estimation of the Choiyoi Magmatic Province and its comparison with other Silicic Large Igneous Provinces. Journal of South American Earth Sciences 103: 102749.
- Beygi, S.; Talovina, I.V.; Tadayon, M.; Pour, A.B. 2020. Alteration and structural features mapping in Kacho-Mesqal zone, Central Iran using ASTER remote sensing data for porphyry copper exploration. International Journal of Image and Data Fusion 12 (2): 155-175.
- Bissig, T.; Lee, J.K.W.; Clark, A.H.; Heather, K.B. 2001. The cenozoic history of volcanism and hydrothermal alteration in the central andean flat-slab region: New ⁴⁰Ar/³⁹Ar constraints from the El indio-pascua Au (-Ag, Cu) belt, 29°20′-30°30′ S. International Geology Review 43 (4): 312-340.
- Busquets, P.; Limarino, C.O.; Cardó, R.; Méndez-Bedia, I.; Gallastegui, G.; Colombo, F.; Heredia, N.; Césari, S.N. 2013. El neopaleozoico de la sierra de castaño (Cordillera Frontal Andina, San Juan, Argentina): Reconstrucción tectónica y paleoambiental. Andean Geology 40 (1): 172-195. doi: http://dx.doi.org/10.5027/andgeoV40n1-a08
- Caballé, M.F. 1986. Estudio geológico del sector oriental de la Cordillera Frontal entre los ríos Manrique y

- Calingasta (Provincia de San Juan). Ph.D. Thesis (Unpublished), Universidad Nacional de La Plata, Facultad de Ciencias Naturales y Museo: 205 p.La Plata
- Caminos, R. 1979. Cordillera Frontal. *In Simposio de Geología Regional Argentina*, No. 2, Volumen I: 397-453. Córdoba.
- Cardó, R.; Díaz, I.N.; Cegarra, M.; Heredia, N.; Rodríguez Fernández, R.; Santamaría, G. 2005. Hoja Geológica 3169-I, Rodeo. Provincia de San Juan. Instituto de Geología y Recursos Minerales. Servicio Geológico Minero Argentino, Boletín 272: 47 p., mapa escala 1:250.000. Buenos Aires.
- Castillo Herrera, D.E. 2021. Petrografía y análisis de facies de rocas estratificadas del Guadalupiano-Triásico medio en la Cordillera Frontal de Elqui (29°58'-30°24' S), Región de Coquimbo, Chile. Ph.D. Thesis (Unpublished), Universidad de Concepción: 220 p. Concepción.
- Charchaflié, D. 1994. Geología del tramo medio y superior de la Quebrada Chita (Provincia de San Juan). Trabajo final de licenciatura (Unpublished), Universidad Nacional de Buenos Aires: 100 p.
- Cócola, M.A.; D'Annunzio, M.C.; Rodríguez, M.E.; Strazzere, L.; Guido, D.M. 2022. Caracterización de las asociaciones de alteración hidrotermal mediante el uso de imágenes ASTER y espectroscopía de reflectancia de infrarojo en el distrito minero Castaño Nuevo, San Juan. *In* Congreso Geológico Argentino, No. 21, Actas: 653-654. Puerto Madryn.
- Coloma, F.; Valin, X.; Oliveros, V.; Vásquez, P.; Creixell, C.; Salazar, E.; Ducea, M.N. 2017. Geochemistry of Permian to Triassic igneous rocks from northern Chile (28°-30°15'S): Implications on the dynamics of the proto-Andean margin. Andean Geology 44 (2): 147-178. doi: http://dx.doi.org/10.5027/andgeoV44n2-a03
- Congalton, R.; Green, K. 2019. Assessing the Accuracy of Remotely Sensed Data: Principles and Practices. Third edit. CRC Press: 1-347. New York.
- Congedo, L. 2021. Semi-Automatic Classification Plugin: A Python tool for the download and processing of remote sensing images in QGIS. Journal of Open Source Software 6 (64): 3172.
- Davidson, J.; Mpodozis, C. 1991. Regional geologic setting of epithermal gold deposits, Chile. Economic Geology 86 (6): 1174-1186.
- del Rey, A.; Deckart, K.; Planavsky, N.; Arriagada, C.; Martínez, F. 2019. Tectonic evolution of the southwestern margin of Pangea and its global implications: Evidence from the mid Permian-Triassic magmatism along the

- Chilean-Argentine border. Gondwana Research 76: 303-321
- Delendatti, G.L. 2003. Caracterización de zonas de alteración hidrothermal en las márgenes del río Castaño, provincia de San Juan, mediante procesamiento digital de imágenes TM. Revista de la Asociación Geológica Argentina 58 (1): 97-108.
- Di Tommaso, I.; Rubinstein, N. 2007. Hydrothermal alteration mapping using ASTER data in the Infiernillo porphyry deposit, Argentina. Ore Geology Reviews 32 (1-2): 275-290.
- Espina, R.G.; Cegarra, M.I.; Ragona, D. 1998. Hoja 3169-20 Castaño Nuevo, Provincia de San Juan. Instituto de Geología y Recursos Minerales. Servicio Geológico Minero Argentino, Boletín 282: 81 p., mapa escala 1:100.000. Buenos Aires.
- Furque, G. 1962. Perfil geológico de la Cordillera de Olivares, Iglesia, San Juan. *In Primeras Jornadas* Geológicas Argentinas, Anales 2: 79-88. Buenos Aires.
- Giambiagi, L.; Álvarez, P.P.; Creixell, C.; Mardónez, D.; Murillo, I.; Velásquez, R.; Lossada, A.; Suriano, J.; Mescua, J.; Barrionuevo, M. 2017. Cenozoic Shift From Compression to Strike-Slip Stress Regime in the High Andes at 30°S, During the Shallowing of the Slab: Implications for the El Indio/Tambo Mineral District. Tectonics 36 (11): 2714-2735.
- Gianni, G.M.; Navarrete, C.R. 2022. Catastrophic slab loss in southwestern Pangea preserved in the mantle and igneous record. Nature Communications 13: 698.
- Gutiérrez, P.R. 1983. Geología del tramo medio de la Quebrada de Agua Negra, Departamento de Iglesias, Provincia de San Juan. Ph.D. Thesis (Unpublished), Universidad Nacional de Buenos Aires: 190 p.
- Heredia, N.; Rodríguez Fernández, L.R.; Gallastegui, G.; Busquets, P.; Colombo, F. 2002. Geological setting of the Argentine Frontal Cordillera in the flat-slab segment (30°00′-31°30′S latitude). Journal of South American Earth Sciences 15 (1): 79-99.
- Hosseini Nasab, M.; Agah, A. 2023. Mapping Hydrothermal Alteration Zones Associated with Copper Mineralization using ASTER Data: A Case Study from the Mirjaveh Area, Southeast Iran. International Journal of Engineering 36 (4): 720-732.
- Jones, R.E.; Kirstein, L.A.; Kasemann, S.A.; Litvak, V.D.; Poma, S.; Alonso, R.N.; Hinton, R. 2016. The role of changing geodynamics in the progressive contamination of Late Cretaceous to Late Miocene arc magmas in the southern Central Andes. Lithos 262: 169-191.
- Kamel, M.; Tolba, A.; AbuBakr, M.M.; Omar, M.M. 2022. Utilization of Landsat-8 data for lithological mapping

- of neoproterozoic basement rocks in north Qena-Safaga road, North Eastern Desert, Egypt. Journal of African Earth Sciences 186: 104420.
- Kleiman, L.E.; Japas, M.S. 2009. The Choiyoi volcanic province at 34°S-36°S (San Rafael, Mendoza, Argentina): Implications for the Late Palaeozoic evolution of the southwestern margin of Gondwana. Tectonophysics 473 (3-4): 283-299.
- Llambías, E.J.; Sato, A.M. 1990. El Batolito de Colangüil (29°-31°S) Cordillera Frontal de Argentina: Estructura y marco tectónico. Revista Geológica de Chile 17 (1): 89-108.
- Llambías, E.J.; Sato, A.M. 1995. El batolito de Colangüil: Transición entre orogénesis y anorogénesis. Revista de la Asociación Geológica Argentina 50 (1-4): 111-131.
- Maksaev, V.; Moscoso, R.; Mpodozis, C.; Nasi, C. 1984. Las unidades volcánicas y plutónicas del Cenozoico Superior en la Alta Cordillera del Norte Chico (29°-31°S): geología, alteración hidrotermal y mineralización. Revista Geológica de Chile 21: 11-51.
- Mars, J.C.; Rowan, L.C. 2006. Regional mapping of phyllicand argillic-altered rocks in the zagros magmatic arc, Iran, using advanced spaceborne thermal emission and reflection radiometer (ASTER) data and logical operator algorithms. Geosphere 2 (3): 161-186.
- Mars, J.C.; Rowan, L.C. 2010. Spectral assessment of new ASTER SWIR surface reflectance data products for spectroscopic mapping of rocks and minerals. Remote Sensing of Environment 114 (9): 2011-2025.
- Martínez, F.; Arriagada, C.; Valdivia, R.; Deckart, K.; Peña, M. 2015. Geometry and kinematics of the Andean thick-skinned thrust systems: Insights from the Chilean Frontal Cordillera (28°-28.5°S), Central Andes. Journal of South American Earth Sciences 64: 307-324.
- Martínez, F.; Arriagada, C.; Bascuñán, S. 2018. Mechanisms and Episodes of Deformation Along the Chilean-Pampean Flat-Slab Subduction Segment of the Central Andes in Northern Chile. *In* The Evolution of the Chilean-Argentinean Andes (Folguera, A.; Contreras-Reyes, E.; Heredia, N.; Encinas, A.; Iannelli, S.; Oliveros, V.; Dávila, F.; Collo, G.; Giambiagi, L.; Maksymowicz, A.; Iglesia Llanos, M.P.; Turienzo, M.; Naipauer, M.; Orts, D.; Litvak, V.; Álvarez, O.; Arriagada, C.; editors). Springer Earth System Sciences: 273-290. Cham.
- Marzouki, A.; Dridri, A. 2023. Lithological discrimination and structural lineaments extraction using Landsat 8 and ASTER data: a case study of Tiwit (Anti-Atlas, Morocco). Environmental Earth Sciences 82 (5): 1-17.

- Massironi, M.; Bertoldi, L.; Calafa, P.; Visonà, D.; Bistacchi, A.; Giardino, C.; Schiavo, A. 2008. Interpretation and processing of ASTER data for geological mapping and granitoids detection in the Saghro massif (eastern Anti-Atlas, Morocco). Geosphere 4 (4): 736-759.
- Moscoso, R.; Mpodozis, C. 1988. Estilos Estructurales en el Norte Chico de Chile (28°-31°S), Regiones de Atacama y Coquimbo. Revista Geológica de Chile 15 (2): 151-166.
- Mpodozis, C.M.; Cornejo, P.P. 1986. Hoja Pisco Elqui, región de Coquimbo. Servicio Nacional de Geología y Minería. Carta Geológica de Chile 68: 164 p., 1 mapa escala 1:250.000. Santiago.
- Mpodozis, C.; Ramos, V.A. 1989. The Andes of Chile and Argentina. *In* Geology of the Andes and its Relation to Hidrocarbon and Mineral Resources (Ericksen, G.E.; Cañas Pinochet, M.T.; Reinemund, J.A.; editors). Circum-Pacific Council: 59-90. Houston, Texas.
- Mpodozis, C.M.; Kay, S.M. 1990. Provincias magmáticas ácidas y evolución tectónica de Gondwana: Andes Chilenos (28-31°S). Revista Geológica de Chile 17 (2): 153-180.
- Mpodozis, C.; Kay, S.M. 1992. Late Paleozoic to Triassic evolution of the Gondwana margin: evidence from Chilean Frontal cordilleran batholiths (28°S to 31°S). Geological Society of America Bulletin 104 (8): 999-1014.
- Murillo, I.R.; Velásquez, R.H.; Creixell, C.T. 2017. Geología de las áreas Guanta-Los Cuartitos y Paso de Vacas Heladas, regiones de Atacama y Coquimbo. Servicio Nacional de Geología y Minería, Carta Geológica de Chile, Serie Geología Básica 192-193: 96 p., 1 mapa escala 1:100.000. Santiago.
- Ninomiya, Y.; Fu, B.; Cudahy, T.J. 2005. Detecting lithology with Advanced Spaceborne Thermal Emission and Reflection Radiometer (ASTER) multispectral thermal infrared "radiance-at-sensor" data. Remote Sensing of Environment 99 (1-2): 127-139.
- Oliveros, V.; Vásquez, P.; Creixell, C.; Lucassen, F.; Ducea, M.N.; Ciocca, I.; González, J.; Espinoza, M.; Salazar, E.; Coloma, F.; Kasemann, S.A. 2020. Lithospheric evolution of the Pre- and Early Andean convergent margin, Chile. Gondwana Research 80: 202-227.
- Olofsson, P.; Foody, G.M.; Herold, M.; Stehman, S.V.; Woodcock, C.E.; Wulder, M.A. 2014. Good practices for estimating area and assessing accuracy of land change. Remote Sensing of Environment 148: 42-57.
- Ouhoussa, L.; Ghafiri, A.; Aissi, L. Ben; Es-Sabbar, B. 2023. Integrating Aster Images Processing and Fieldwork for Identification of Hydrothermal Alteration Zones

- at the Oumjrane-Boukerzia District, Moroccan Anti-Atlas. Open Journal of Geology 13 (02): 171-188.
- Ourhzif, Z.; Algouti, A.; Algouti, A.; Hadach, F. 2019. Lithological mapping using Landsat 8 OLI and ASTER multispectral data in Imini-Ounilla District South Atlas of Marrakech. International Archives of the Photogrammetry, Remote Sensing and Spatial Information Sciences XLII-2W13, 1255-1262.
- Perelló, J.; Sillitoe, R.H.; Rossello, J.; Forestier, J.; Merino, G.; Charchaflié, D. 2023. Geology of Porphyry Cu-Au and Epithermal Cu-Au-Ag Mineralization at Filo del Sol, Argentina-Chile: Extreme Telescoping During Andean Uplift. Economic Geology 118 (6): 1261-1290.
- Pérez, D.J.; D'Odorico Benites, P.E.; Godeas, M.C. 2010. Reconocimiento de alteración hidrotermal con el sensor ASTER, en el curso medio del Río Santa Cruz (31°40'S), provincia de San Juan. Revista de la Asociación Geológica Argentina 66 (4): 623-633.
- Polanski, J. 1970. Carbónico y Pérmico de la Argentina. Eudeba: 215 p. Buenos Aires.
- Poma, S.; Ramos, A.; Litvak, V.D.; Quenardelle, S.; Maisonnave, E.B.; Díaz, I. 2017. Southern Central Andes Neogene magmatism over the Pampean Flat Slab: implications on crustal and slab melts contribution to magma generation in Precordillera, Western Argentina. Andean Geology 44 (3): 249-274. doi: http://dx.doi.org/10.5027/andgeoV44n3-a02
- Pour, A.B.; Hashim, M.; Hong, J.K.; Park, Y. 2019. Lithological and alteration mineral mapping in poorly exposed lithologies using Landsat-8 and ASTER satellite data: North-eastern Graham Land, Antarctic Peninsula. Ore Geology Reviews 54 (108): 181-196.
- Ramos, V.A. 1999. Rasgos estructurales del territorio argentino. *In* Geología Argentina (Caminos, R.; editor). Instituto de Geología y Recursos Minerales: 15-75. Buenos Aires.
- Richards, J.A.; Jia, X. 2006. Remote Sensing Digital Image Analysis: An Introduction. 4th edition. Springer: 439 p. Berlin.
- Rocher, S.; Vallecillo, G. 2014. Mecanismos eruptivos y procesos depositacionales del Grupo Choiyoi en el área de Las Caletas, Cordillera Frontal de San Juan, Argentina. Andean Geology 41 (3): 589-625.
- Rocher, S.; Vallecillo, G.; Castro de Machuca, B.; Alasino, P. 2015. El Grupo Choiyoi (Pérmico temprano-medio) en la Cordillera Frontal de Calingasta, San Juan, Argentina: volcanismo de arco asociado a extensión. Revista Mexicana de Ciencias Geológicas 32 (3): 415-432.

- Rodríguez Fernández, L.R.; Heredia, N.; Gallastegui, G.; Quesada, C.; Robador, A. 1996. Hoja 3169-20 Castaño Nuevo, Provincia de San Juan. Instituto de Geología y Recursos Minerales. Servicio Geológico Minero Argentino, Boletín 329: 145 p., mapa escala 1:100.000. Buenos Aires.
- Rodríguez Fernández, L.R.; Heredia, N.; Espina, R.G.; Cegarra, M. 1999. Estratigrafía y estructura de los Andes Centrales Argentinos entre los 30° y 31° de Latitud Sur. Acta Geológica Hipánica 32: 51-75.
- Rowan, L.C.; Mars, J.C. 2003. Lithologic mapping in the Mountain Pass, California area using Advanced Spaceborne Thermal Emission and Reflection Radiometer (ASTER) data. Remote Sensing of Environment 84 (3): 350-366.
- Salazar, E.; Coloma, F. 2016. Geología del área Cerros de Cantaritos-Laguna Chica, región de Atacama.
 Servicio Nacional de Geología y Minería, Carta Geológica de Chile, Serie Geología Básica 181: 171 p., 1 mapa escala 1:100.000. Santiago.
- Sato, A.M.; Llambías, E.J. 1993. El Grupo Choiyoi, provincia de San Juan: equivalente efusivo del Batolito de Colangüi. *In* Congreso Geológico Argentino, No. 12, y Congreso de Exploración de Hidrocarburos, No. 2, Actas 4: 156-165. Mendoza.
- Sato, A.M.; Llambías, E.J.; Basei, M.A.S.; Castro, C.E. 2015. Three stages in the Late Paleozoic to Triassic magmatism of southwestern Gondwana, and the relationships with the volcanogenic events in coeval basins. Journal of South American Earth Sciences 63: 48-69.
- Sillitoe, R.H. 1977. Permo-Carboniferous, upper Cretaceous, and Miocene porphyry copper-type mineralization in the Argentinian Andes. Economic Geology 72 (1): 99-103.

- Spalletti, L.A.; Limarino, C.O.; Piñol, F.C. 2012. Petrology and geochemistry of Carboniferous siliciclastics from the Argentine Frontal Cordillera: A test of methods for interpreting provenance and tectonic setting. Journal of South American Earth Sciences 36: 32-54.
- Testa, F.J.; Villanueva, C.; Cooke, D.R.; Zhang, L. 2018. Lithological and hydrothermal alteration mapping of epithermal, porphyry and tourmaline breccia districts in the Argentine Andes using ASTER imagery. Remote Sensing 10 (2): 1-45.
- Velásquez, R.H.; Coloma, F.B.; Murillo, I.R.; Merino, R.G.; Ortiz, M.L. 2021. Geología de las áreas Pisco Elqui y Paso del Agua Negra, región de Coquimbo. Servicio Nacional de Geología y Minería, Carta Geológica de Chile, Serie Geología Básica 211-212: 201 p., 1 mapa escala 1:100.000. Santiago.
- Vitaller, A. 1994. Descripción Geológica de la región de las nacientes del Arroyo de Chita (Provincia de San Juan). Trabajo final de licenciatura (Inédito), Universidad Nacional de Buenos Aires: 92 p. Buenos Aires.
- Watts, D.R.; Harris, N.B.W.; Gaines, J.S.; Ishmael, C.L.; Larsen, K.A.; May, D.Z.; Roberts, S.P.; Rogers, J.; Steger, D.B.; Sullivan, M.T. 2005. Mapping granite and gneiss in domes along the North Himalayan antiform with ASTER SWIR band ratios. Bulletin of the Geological Society of America 117 (7-8): 879-886.
- Wetten, A.F. 2005. Andesita Cerro Bola: Nueva unidad vinculada al magmatismo mioceno de la Cordillera de Olivares, San Juan, Argentina (30°35′S; 69°30′O). Revista de la Asociación Geológica Argentina 60: 3-8.
- Yamaguchi, Y.; Kahle, A.B.; Tsu, H.; Kawakami, T.; Pniel, M. 1998. Overview of advanced spaceborne thermal emission and reflection radiometer (ASTER). IEEE Transactions on Geoscience and Remote Sensing 36 (4): 1062-1071.

Supplementary Material

Aster bands resampling

When ASTER processing includes both the 15 m resolution VNIR bands and the 30 m resolution SWIR bands, it is necessary to convert the data to a common spatial resolution. This conversion is made through raster resampling. In this study, we use the **nearest neighbor method**, which calculates the value of each cell in the output raster using the value of the nearest cell in the input raster. The nearest neighbor resampling method preserves the values of cells from the input layer, without making any averaging or smoothing, and for this reason it is a recommended option for working with remote sensing data (Jensen, 2015).

There are two options to achieve a common resolution for VNIR and SWIR data: **magnify** the SWIR bands to 15 m/pixel, to fit with VNIR data, or **reduce** the resolution of VNIR bands to 30 m/pixel. In the literature, previous works that use ASTER data for geological studies employ both methodologies. For instance, Massironi *et al.* (2008), Testa *et al.* (2018), Baid *et al.* (2023), and Hosseini Nasab and Agah (2023) use magnification, while Di Tommaso and Rubinstein (2007), and Ourhzif *et al.* (2019) prefer reduction.

To examine the effects of nearest neighbor resampling to lower and higher resolutions, we conducted a short exercise with VNIR and SWIR bands from the same ASTER scene, acquired on March 14, 2002. Band 7 with 30 m of resolution was resampled to 15 m, while band 3 with 15 m of resolution was resampled to 30 m. In the first case, each 30x30 m pixel in the original raster image was replaced by four 15x15 m pixels, all with the same value as the original input pixel. In the second case, each newly created 30x30 pixel takes one of the values from the four original 15x15 pixels.

After resampling, we compared each original raster with its resampled equivalent (Fig. A). When we compared the original band 7 (30 m/pixel) with the resampled one (15 m/pixel), the subtraction of the two raster files gives 0 in the whole image. On the other hand, when resampled band 3 (30 m/pixel) is compared with the original raster (15 m/pixel), the two rasters exhibited differences in reflectance values up to 0.38, which is expected because there is an obvious loss of detail.

These results lead us to the conclusion that resampling to higher resolution (this is, resample the 30 m resolution SWIR bands to the 15 m resolution VNIR bands) does not affect the properties of the output raster image and, in consequence, land surface properties. In addition, this approach allows us to benefit from the higher spatial resolution of the VNIR bands during ASTER processing. The disadvantage is that magnification of SWIR bands introduces a false sense of accuracy, related to the creation of new pixels which simply assume a value from the input raster. However, because in ASTER processing combined bands are from the same ASTER scene, we should expect that this "assumption" will not affect the ASTER processing results.

Some authors consider as a good practice to resample at the lowest resolution when working with raster data. This more conservative approach avoids the problem of generating a "false resolution" associated with the creation of new pixels. However, this implies the loss of information from VNIR bands, and the modification of the land surface properties, as we demonstrated in our exercise (Fig. A).

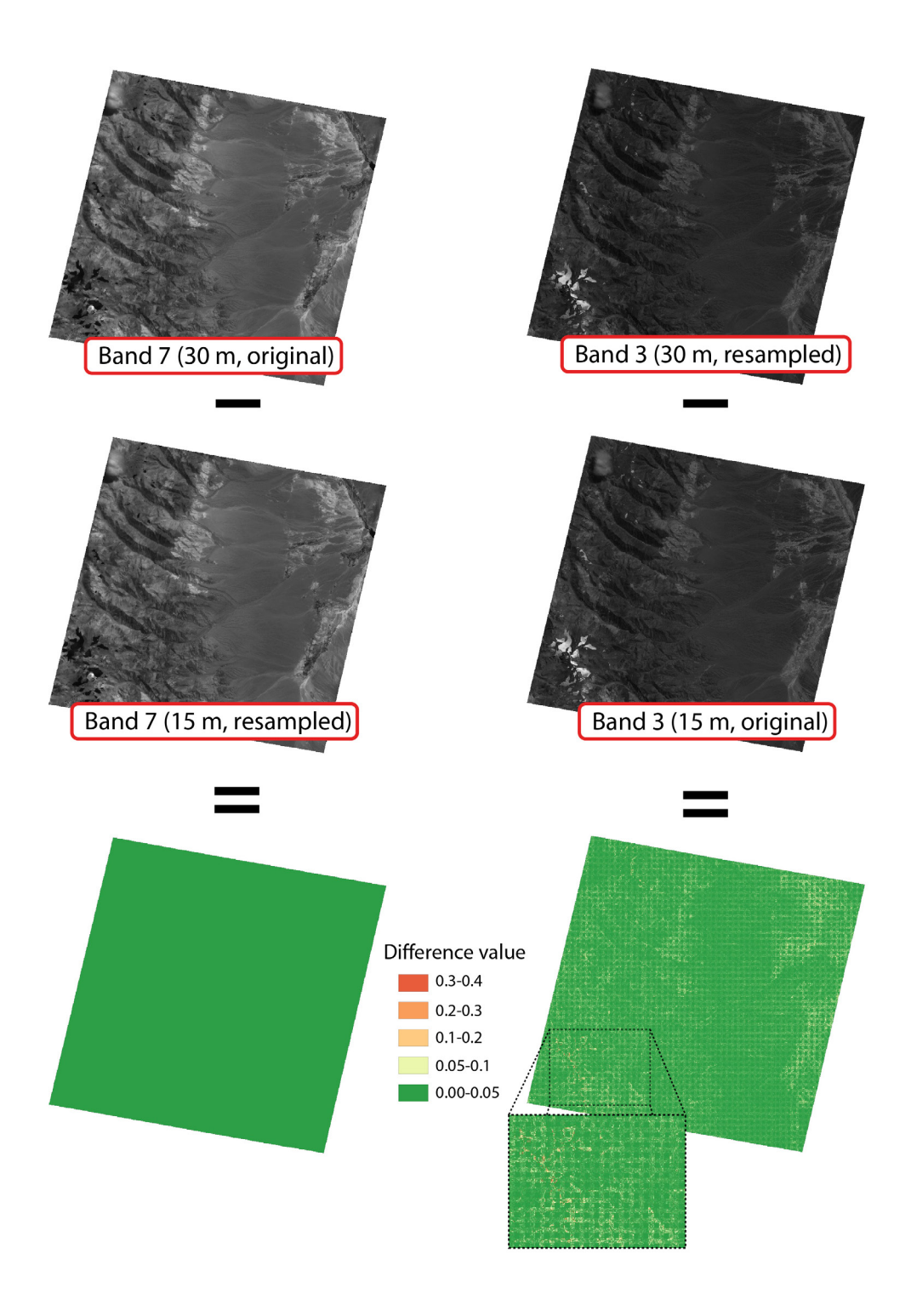


FIG. A. Subtraction operations made with original and resampled VNIR and SWIR bands. The output raster shows the absolute difference values between the 15 m and 30 m resolution rasters for ASTER bands 3 and 7. Note that, when resampling to 15 m of resolution, the reflectance values do not change in the whole image.

Based on this analysis, we resample the SWIR bands to 15 m resolution. We believe the magnification of SWIR bands does not negatively impact ASTER processing, and that this approach allows a better use of the VNIR data.

References

- Baid, S.; Tabit, A.; Algouti, A.; Algouti, A.; Nafouri, I.; Souddi, S.; Aboulfaraj, A.; Ezzahzi, S.; Elghouat, A. 2023. Lithological discrimination and mineralogical mapping using Landsat-8 OLI and ASTER remote sensing data: Igoudrane region, jbel saghro, Anti Atlas, Morocco. Heliyon 9 (7): e17363.
- Di Tommaso, I.; Rubinstein, N. 2007. Hydrothermal alteration mapping using ASTER data in the Infiernillo porphyry deposit, Argentina. Ore Geology Reviews 32 (1-2): 275-290.
- Hosseini Nasab, M.; Agah, A. 2023. Mapping Hydrothermal Alteration Zones Associated with Copper Mineralization using ASTER Data: A Case Study from the Mirjaveh Area, Southeast Iran. International Journal of Engineering 36 (4): 720-732.
- Jensen, J.R. 2015. Introductory Digital Image Processing: A Remote Sensing Perspective. 4th edition (Botting, C.; editor). Pearson: 623 p. Glenview.
- Massironi, M.; Bertoldi, L.; Calafa, P.; Visonà, D.; Bistacchi, A.; Giardino, C.; Schiavo, A. 2008. Interpretation and processing of ASTER data for geological mapping and granitoids detection in the Saghro massif (eastern Anti-Atlas, Morocco). Geosphere 4 (4): 736-759.
- Ourhzif, Z.; Algouti, A.; Algouti, A.; Hadach, F. 2019. Lithological mapping using landsat 8 oli and aster multispectral data in imini-ounilla district south high atlas of marrakech. International Archives of the Photogrammetry, Remote Sensing and Spatial Information Sciences XLII-2W13, 1255-1262.
- Testa, F.J.; Villanueva, C.; Cooke, D.R.; Zhang, L. 2018. Lithological and hydrothermal alteration mapping of epithermal, porphyry and tourmaline breccia districts in the Argentine Andes using ASTER imagery. Remote Sensing 10 (2): 1-45.